

AAAF Paper #39-2

DA VINCI X-PRIZE SPACE PROJECT – MISSION ANALYSIS

Vladimir Kudriavtsev¹

CFD Canada, da Vinci Project
vvk@cfdcanada.com

Brian Feeney²

da Vinci Project, ORVA Inc.
bfeeney@davinciproject.com

Max Buneta

da Vinci Project, ORVA Inc.
System Analysis & Design

James Porcher

da Vinci Project, ORVA Inc.
Ground Operations

Asier Ania

da Vinci Project, ORVA Inc.
Thermal Analyst

Michael Trauttmansdorff

da Vinci Project, ORVA Inc.
System Design and CAD

Ta-Liang Hsu

da Vinci Project, ORVA Inc.
Stress Analyst

Marek Krzeminski

da Vinci Project, ORVA Inc.
Dynamics and Control

Kalman Rooz

da Vinci Polytechnic Institute
Senior Consultant

ABSTRACT

In the present article we review engineering and research efforts conducted by a group of volunteers with the help of advanced engineering commercial software (CFD-ACE+, ANSYS, CFD-FASTRAN, Matlab/Simulink, Autodesk Inventor, Maple) in support of the da Vinci Project, the first Canadian competitor in the International X Prize Competition. The da Vinci Project has an objective of launching the first commercial sub-orbital manned space flight by 2004. Under X Prize rules the vehicle must be reusable, built to hold 3 people and complete 2 flights within a 2 week period. The basic launch configuration is to lift the rocket using a reusable helium balloon to a launch altitude of 24,400 meters (80,000 feet).

The paper describes in detail the various major subsystem components of the Rocket, Balloon Launch Platform, Ground Operations and Logistics and the multidisciplinary approach to arrive at a viable and safe design. A state of the art software and engineering data management methodology is described. All parameters that effect the design are ported through a data management software linking, CFD, FEA and Flight Simulation software's directly to the primary CAD platform resulting in direct updates to the CAD model. This process allows an iterative design to develop rapidly, multiple configurations to be assessed and a final design output in the shortest overall timeframe. The data management software contains every parameter in the rockets design including all rocket engine performance criteria. Running a variation on the engine Isp (Specific Impulse) results in the CAD drawings updated with new tank sizes etc, yet still driven by constrictions such as maximum diameter of the vehicle. Lowering of the Isp in such case would result in the need for more fuel to reach the minimum assigned altitude of 115 Kms. The rockets length would automatically be increased, given a diameter restriction. CG and CP values for instance are automatically recalculated for stability analysis.

¹ Ph.D. AE, Member CASI, AIAA, ASME, R&D Team Lead, <http://www.cfdcanada.com>

² Corresponding author, da Vinci Project Team Lead, <http://www.davinciproject.com>

1. INTRODUCTION

1.1 X-prize

The da Vinci Project™ is the first Canadian entry in the X-Prize Competition, the international “New Race to Space®” [1]. The purpose of the X-Prize is to promote the development and flight of spacecraft able to provide low-cost commercial transport of humans into space [2-7]. The X-prize Foundation is providing a purse of US\$ 10 million to the first competitor who can safely launch and land a manned spacecraft to an altitude of 100 kilometers, twice in a two-week period. The X Prize parallels the Orteig Prize won by Charles Lindbergh in 1927. The day before Charles Lindbergh flew, a 40-passenger clipper class flying boat was inconceivable. Where's the technology? You'll never be able to finance it! Less than 7 years later the flying boats were gracing the sky's of the larger Pacific let alone the Atlantic. We face a similar challenge of the mind today.

The X-Prize competition is opening up space for the average person. Not just literally providing them with a more cost effective way of getting to space, but breaking down the psychological barriers that have built up through the past decades. The crux of this goal is to inspire through "actions" a new generation of forward thinking youth. Show them just as Lindbergh did in 1927 that the seemingly impossible can be done. This applies not only to space but also to the broader challenges and opportunities we face in life. There are a great many opportunities and rewards that this unique project will develop. The da Vinci Project's objectives are capturing the X Prize and delivering a reusable spacecraft and safe low cost launching system. The da Vinci Project has already made history. In early March of 2003 the da Vinci Project became first in the private sector to make an official application to government for approval to launch a manned rocket into space. The application was submitted following a project review with the Canadian Government Ministry of Transport and the CLSO (Canadian Launch Safety Office). The application was well received and is being processed toward approval.

Several technologies will be demonstrated over successive flights including greater than 90% reusability of flight hardware, short turn around time, minimum logistical and launch support, first approved civilian manned launch permit to space, low project and recurring costs, demonstrated ability to work with government and the National Transportation System, aircraft FAR engineering approach to design, manufacturing and system redundancy – safety.

A core of over 200 professionals volunteer their contributions and more than 35 corporate technical sponsors back the project. Aerospace engineers, experts in project management, finance, media, public relations and graphic design volunteer their time and expertise towards the realization of the next step in Human discovery [5,7]. The da Vinci Project's novel rocket design will be launched from the world's largest reusable helium balloon at an altitude of 80,000 feet (24,400 meters).

1.2 Testing and Development

The da Vinci Project began its vehicle development shortly after the X PRIZE was announced in 1996, with official entry of the team into the competition in 2000. The da Vinci Project is wholly owned by ORVA Space Corp, a Canadian company. Years of engineering research, design and developmental testing has gone into the vehicle design, propulsion and flight guidance system (see Figs. 1(a-c),2(a-c)). The da Vinci Project has teamed up with one of North America's leading Aerospace Rocket Propulsion companies to build the final flight configuration engines.

The da Vinci Project employs an aircraft “FAR” engineering approach to design, manufacturing and system redundancy – safety. This approach basically says that the primary objective of any flight is the safety of the flight crew and of civilian populations. The approach therefore is to always be in a position to lose and or abort a mission without loss of the vehicle or it's crew. Propulsion systems design and performance criteria as well as overall systems architecture were selected to deliberately favor this critical. Loss of engine power can take place at any point in the launch sequence followed by abort to re-entry, recovery mode and full recovery of the capsule and propulsion sections.



Figure 1a. Engineering prototype (full scale)



Figure 1b. Aeroshell



Figure 1c. Transportation of engineering prototype

A full-scale flight-engineering prototype of the manned rocket has been constructed (Fig. 1a). Detailed engineering and fabrication of the full-scaled manned rocket named Wild Fire Mk VI™ is currently underway. Flight-testing of the manned rocket and X Prize Competition flights are targeted to start in late 2003 and continue throughout 2004.

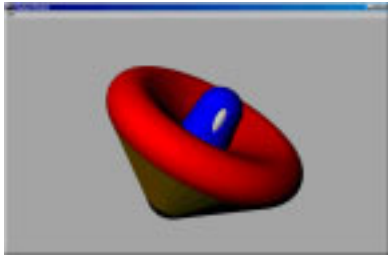


Figure 2a. Ballute concept (subsequently discarded in favor of separate re-entry)



Figure 2b. Rocket Block (for ballute concept)

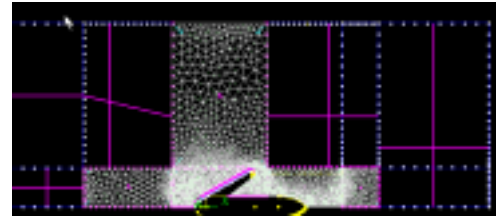


Figure 2c. Computational setup for ballute aerodynamic analysis (using CFD-ACE+)

2. SYSTEM LEVEL MISSION ANALYSIS AND INTEGRATION APPROACH

In this article we will review some of the key aspects of the da Vinci space program and main components of the mission profile. We will identify and analyze key research topics required for successful design. This includes base trajectory analysis, aeroheating analysis during re-entry, spacecraft external and internal aerodynamics and heating, transient thermal analysis of thermal protection, spacecraft stress analysis, balloon trajectory and launch considerations, parachute system deployment, trajectory dynamics and control. We will also briefly discuss engineering integration of our research efforts with the CAD design process. For R&D efforts presented in this paper we utilized Maple mathematics software package for basic engineering calculations, Matlab /Simulink for advanced trajectory analysis, dynamics and mission control, FASTRAN and CFD-ACE+ software package for supersonic external aerodynamics (Fig. 2c), internal flows and heating, ANSYS for structural stress analysis and thermal analysis of TPS, Inventor package for all CAD work and geometry creation. Our main engineering approach was to identify potential problem areas, study them in detail using available computational tools and to develop corresponding design solutions.

2.1 Introduction and Overview

The spacecraft which the da Vinci team is currently producing has been christened the Wild Fire Mk VI™, and is the latest in a series of designs that have been revised and updated over the years of the team's existence (Figs.1(a-c),2(a-c)). Originally envisioned as a single component balloon launched vehicle (Fig. 1a), returning to earth using a conical ballute (Fig. 2a), the design has transformed considerably since its beginnings around the year 2000.

The strategy that has been chosen still features the original concept of a small spacecraft undertaking airborne launch at high altitude from a balloon. However, our reentry plan has been changed to increase the level of passive safety built into the design, and to move away from the cutting edge ballute design and towards a more conventional parachute and airbag configuration. Return to the earth will be accomplished by the spacecraft separating the manned capsule from the primary propulsion section, and having both sections return to the ground independently of each other. The separability of the propulsion system and the manned capsule adds to the crew safety by providing an escape option at all stages of the mission.

With the spacecraft consisting of two primary subsections, a capsule and a rocket block, it follows the conventional strategy used by most launch platforms. The distinction, inherent in all x-prize competitors' designs, is that the engine block will be fully recovered alongside the manned capsule, rather than being allowed to burn up on re-entry after its purpose has been served.

The combination of recoverability for all parts of the spacecraft, and an innovative launch using a high altitude balloon has produced a very interesting overall design for the da Vinci Project's bid to put a man into space.

2.2 Subsystem Breakdown

The Wild Fire Mk VI™ spacecraft is divided into two primary subsystems; the capsule and the rocket block. The following is a description of their design, functionality, and of how they interact with each other during different phases of the mission. The capsule is positioned upon the rocket block when assembled, with the crew facing in the forward direction of flight (Figure 3a).

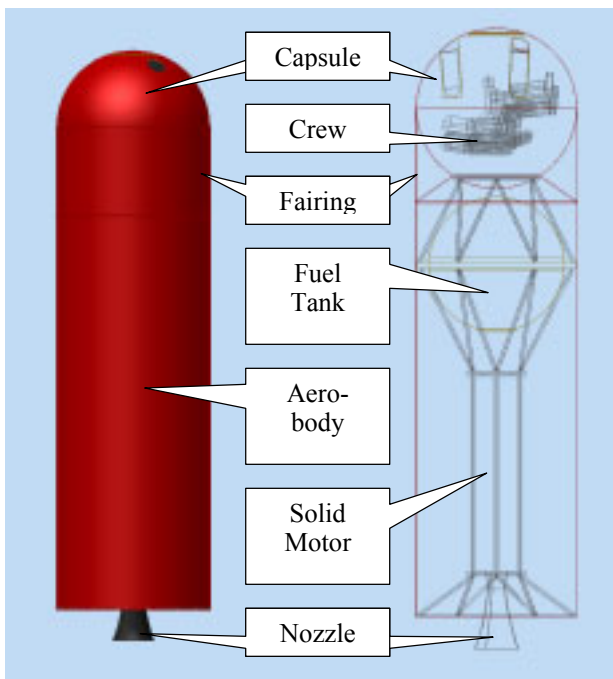


Figure 3a. Assembled Spacecraft

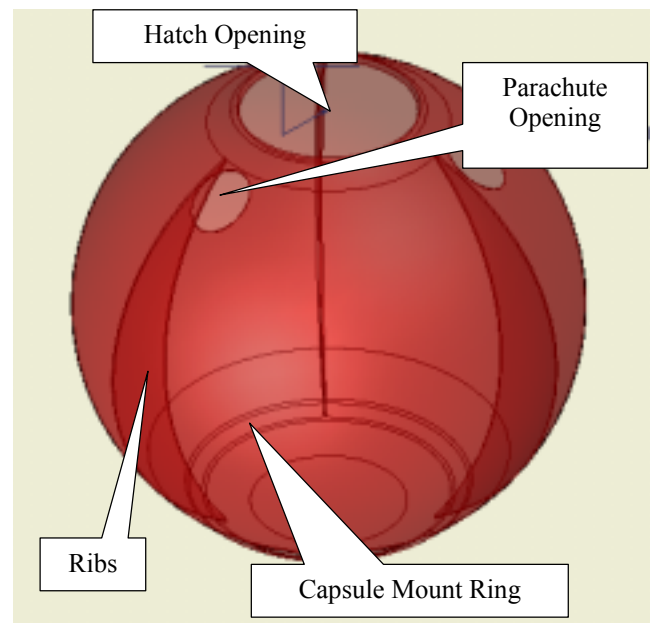


Figure 3b. Capsule Structure

2.2.1 Capsule

The capsule is a spherical body of approximately 2 meter outer diameter. It is being designed as a fully composite structure, made up primarily of Kevlar and fiberglass. The outer skin will be a semi-structural element, with the addition of ribs in the vertical direction for reinforcement. Structural components such as hatch opening ring and parachute mounts will be filament-wound onto the shell, creating an integrated structure. Ribs in the capsule structure will serve several purposes. They provide stiffness for the sphere, to prevent damage resulting from large deformation. The ribs will also be the primary mounting points for subsystems within the capsule, including air tanks and seats. Lastly, they will serve as load transferring members, to distribute the loads from parachute cables to a larger portion of the sphere. (Figure 3b) The base of the capsule will feature a reinforced ‘capsule mounting ring’ which will be paired to a ring on the top of the rocket block. This will serve to mate the two structures during balloon ascent and the launch phase of the flight. Explosive bolts will trigger after the engine has finished firing, and the two modules will be caused to separate by the pressurized airbag housed between them.

The capsule will have a single hatch located at its top at the centerline. It will serve as the means of entry and egress, both during normal operations and emergency escape. The interior of the capsule will feature clearance to permit the rapid escape of the pilot and crew in the event that emergency egress is warranted.

It is desirable to have windows in the final design from the point of view of making the capsule an attractive product. The da Vinci design is known for its many-windowed configuration, and a large part of the appeal of space flight is derived from the idea that the astronauts will see the earth from space. Window housings will be produced in a similar manner to the hatch ring, in that they will be filament wound onto the surface of the shell. This will create a ring of reinforced composite which will hold the window against the internal pressures, as well as providing a thick enough structure for mounting of the window.

The capsule is required to have a capacity of 3 people of 6’ height, within the confines of a 2 meter diameter sphere. This requires a staggered seating configuration, with the pilot somewhat in front of the passengers, and with them close together behind him. The seats themselves will have to provide the necessary level of comfort for the duration of the flight and will also have to cushion the accelerations and impacts which the capsule will undergo. Most importantly, they will feature a pneumatic cushioning mechanism to protect the pilot for harm in the event of an airbag cushion failure.

Flight guidance and control equipment will be inside the cockpit, easily accessible to the pilot. In flight, control inputs will be given by the pilot from armrest mounted joysticks and buttons, which will be useable, even under high g-loads. Of prime importance is the stabilization of the capsule prior to reentry. Despite the passive stabilization that comes from the sphere having a low C/G, orienting the capsule correctly during flight to apogee will reduce the amount of buffeting and other disturbances that would occur as the

capsule rights itself. To accomplish this, the capsule will house a set of RCS thrusters which will be in use both during ascent, to steer the entire spacecraft, and during its ballistic flight to apogee, to stabilize the capsule's orientation and rotation.

A parachute will be used to slow the capsule down from terminal velocity to a safe landing speed of 6m/s. The parachute will be deployed at the maximum possible altitude, to provide the most descent time for the deployment of a backup if the primary parachute fails. In the catastrophic event of both parachutes failing, the crew of the capsule will open the hatch and bail out of the falling capsule, making use of their personal parachutes to achieve safe landings.

Ground approach under parachute is expected to be at 6m/s, and while this is not dangerous to the pilot and crew, it could lead to significant damage to the capsule's structure and equipment. A direct impact with the ground would also cause damage to the thermal protection system on the undersurface of the capsule. In light of our aim to minimize the replacement and repair of components between flights we plan to implement a system of cushioning airbags upon landing, to prevent such damage. The aim of the cushion system is to act as a damper upon landing, and so it would inflate shortly before impact (100m altitude). Upon contact with the ground, air will be forced out and the bags will deflate in a controlled manner, providing a desired level of damping. In the event of airbag failure, capsule damage will occur, but the crew will be protected from injury by the pneumatically cushioned seats. The team is also investigating suppliers and manufacturers for this subsystem, as considerable industry know-how exists in this field, and our design philosophy is to employ proven technologies in all mission critical systems.

2.2.2 Rocket Block

The rocket block is a cylindrical body approximately 5 meters in length, and 2 meters in diameter. Its structure will be an aluminum truss skeleton, designed to transfer all of the axial loads from the engine through to the capsule mount ring. Additional structural rings will be located at the circumference of the fuel tank, at the top and bottom of the solid motor housing, and at the base of the exterior body of the rocket block; the aero-shell. Torsional stiffness will be created by the semi-structural aero-shell and by the angled truss sections. The rings at each of the junctions of the truss form mounting points for the primary propulsion system, and ensure that the entire spacecraft is self supporting.

The primary engine which will propel the spacecraft to its apogee of over 100 km will be a hybrid, using N_2O as the oxidizer, and a fuel grain of Hydroxyl Terminated Poly-Butadiene (HTPB). A hybrid type engine has been selected for its simplicity and high level of safety since both fuels are inert on their own. This minimizes the danger during ground handling. In addition, hybrids have the advantage of allowing the pilot to shut off the engine by cutting off the liquid fuel supply if deemed necessary. Several hundred test firings were performed by our engine supplier (see Figures 4b, c). The engine is in the 68,181 N thrust class (15,000 lbs st) with a total impulse of 4,545,454 Nsec (1,000,000 lbs sec).

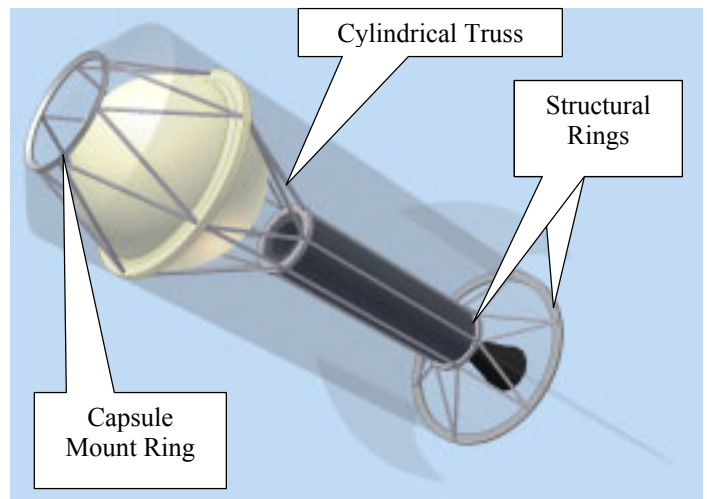


Figure 4a. Rocket block (RB) structure



Figure 4b. Engine Firing Test (8000 lbf class)



Figure 4c. Carbon Fiber Nozzle

Due to the large diameter the Wild Fire Mk VI™ spacecraft, the oxidizer tank will be a spherical pressure vessel, made of filament wound Kevlar to improve its strength to mass ratio. Thermal blankets will protect the tank during balloon ascent to maintain a constant fuel temperature while the spacecraft climbs through ever colder air. The fuel grain will be in a removable housing which will be separated from the spacecraft for replenishment of the HTPB fuel after each flight.

The rocket block will carry its own guidance control and telemetry system, which will be under the pilot's control via a link to the capsule during ascent. Once separation occurs, the rocket block's re-entry systems will be operated in a fully automatic mode, under control of the guidance computer. Steering during the main engine burn will be carried out by the rocket block's RCS a thruster acting in concert with the capsule's set. During ascent to apogee the rocket block will be stabilized and oriented for an ideal descent by its onboard thrusters.

Upon firing of the explosive bolts, and capsule separation, the faring between the two bodies will be cast aside and allowed to burn up on re-entry. The rocket block features a blunt conical nose which has high drag characteristics and will serve to slow the body while it is descending through the atmosphere. The rocket block will descend nose first, stabilized by the fins on the tail end of the spacecraft. Even if the guidance system fails to orient this part of the spacecraft correctly for re-entry, it will stabilize similarly to the V-2 rocket which simply tumbled until there was sufficient dynamic pressure to make its fins effective.

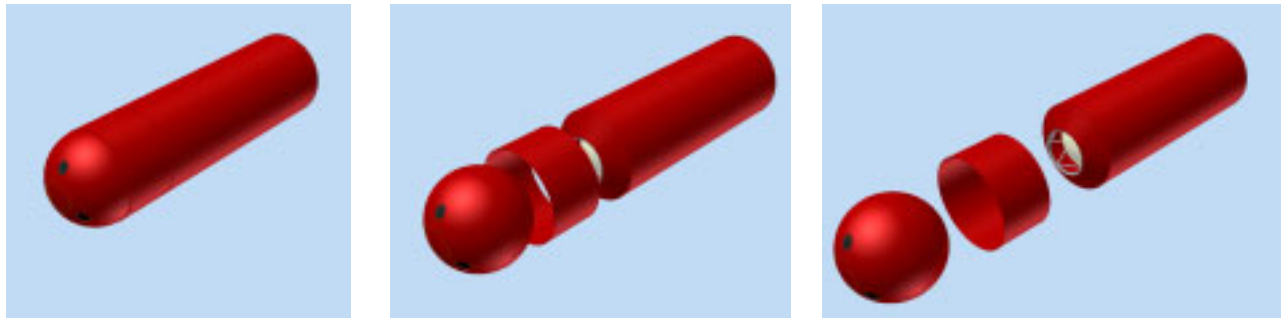


Figure 5. Separation of Capsule from Rocket Block

During descent, the rocket block will be slowed by a parachute deployed from the base of the rocket, and will be suspended for a nose-down landing. To reduce mass, and since there is no crew to protect, a single parachute will suffice for the rocket block.

With a parachute descent speed of 6 m/s, this part of the spacecraft also could still sustain slight damage on landing. The primary structure is intended to take loads in the axial direction, and for this reason a nose down landing is planned. While crew protection is not a concern, the reusability of the craft is paramount, and it will employ an airbag system to reduce the force of landing. This will deploy from under the capsule mount ring. The team is also currently investigating suppliers and manufacturers for this subsystem. Once on the ground, the parachute will be detached, and the rocket block will tip over onto its side.

3. FOCUS AREAS

3.1 Base Trajectory Analysis

In order to facilitate a better understanding of the flight profile, we developed a computer simulation for the trajectory of the launch vehicle and the two re-entry components. The simulator is a useful tool for gauging the performance of the vehicle, as well as providing the design team with a thorough understanding of the critical loads present during the flight. This simulation started as a simple one-dimensional model, tracking the vertical flight path characteristics; it has since grown into a useful 3-d flight modeling tool that also incorporates RCS control, temperature propagation through the skin, and numerous other key characteristics. Computer simulation modeling is in fact an ongoing effort, which will eventually lead to a fully integrated flight control system.

The flight simulator is based on a physics model which takes into account the basic vehicle properties (for example, mass, center of mass, drag coefficients) and the altitude-varying, atmospheric properties (for example, density, pressure, temperature, and wind). Forces affecting the vehicle are re-calculated at user-selected intervals throughout the full flight, usually every 0.1 seconds. The vehicle's acceleration, velocity, and position are updated simultaneously [13,14]. Several numerical algorithms are utilized to integrate system of differential equations of motion. The simulator currently tracks the following sixteen vehicle and flight parameters:

- **Gravitational force**—Calculated according to the International Gravity formula, it varies with altitude and latitude.
- **Thrust force**—Incorporates a time-varying model of engine thrust output as estimated by the manufacturer.
- **Drag force**—Calculated using speed and Re number varying Cd data, vehicle airspeed, and atmospheric conditions.
- **Acceleration:** Determined from the above forces. Acceleration values can be split up into various components for analysis (for example, x, y, z, drag, gravity, thrust).
- **Velocity**—In addition to considering the above accelerations when determining velocity, wind velocity is factored in as well. Again, velocity values may be viewed in their separate components.
- **Position**—The vehicle's position is recorded for every point along its flight.
- **Separation from balloon**—Distance separation between rocket and the spherical balloon, critical during launch.
- **Separation from point of launch**—Distance and directional separation from launch point, critical for landing zone determination.
- **Air temperature**—From the atmospheric data, we track the air temperature at each point in the flight.
- **Skin temperature at stagnation**—Temperatures due to shock-wave are monitored at the point of stagnation (the hottest area) for the re-entry phase of the flight.
- **Temperature propagation through the skin**—A temperature profile through the skin of the vehicle, based on heat conduction.
- **Parachute deployment force**—The force exerted on the vehicle during parachute deployment.
- **Vehicle Mass:** Mass variation due to fuel burn is monitored.
- **Balloon buoyancy force**—The buoyancy force acting on the balloon. Varies with atmospheric conditions.
- **Balloon volume and dimensions**—The volume varies with atmospheric pressure and temperature.
- **Balloon pressure**—Considers atmospheric conditions and rate at which He is vented to outside.

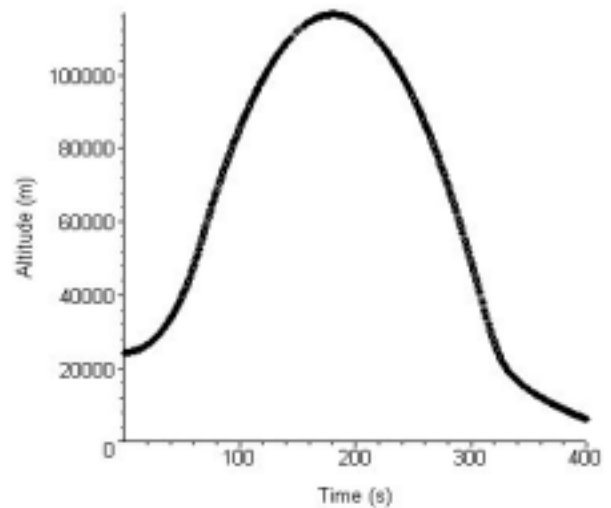


Figure 6. Ballistic Flight Profile

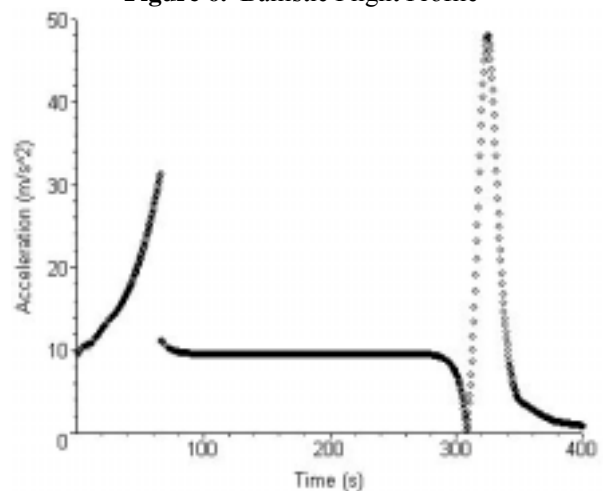


Figure 7. Acceleration profile

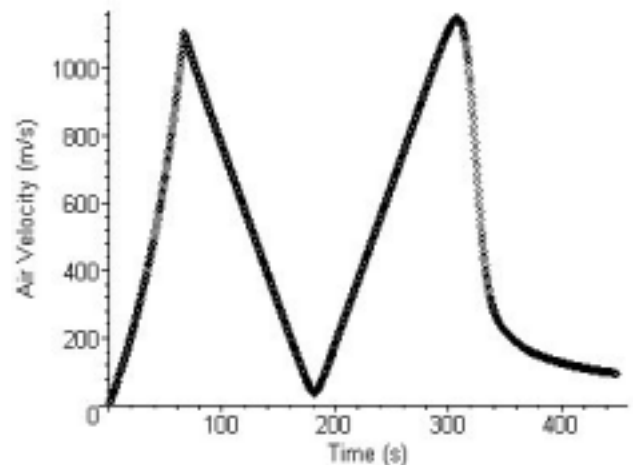


Figure 8. Velocity Profile

The flight trajectory follows a ballistic profile, reaching a maximum altitude of 116km, and then immediately falling back down to Earth (Figure 6). The total flight time, not counting the balloon ascent, is 25 minutes, 18 of which are spent under the parachute. Our engines cut out after 66 seconds, leaving the capsule in free fall after that point. The time in space is therefore relatively short, with only two minutes being spent above the X Prize regulated 100km altitude. The passengers spend about 3.8 minutes in a weightless environment. This is the time between engine cut-off and re-entry into the atmosphere.

The actual time spent under load is quite critical, both for the structural design of the spacecraft and for the occupants within. The simulator gives us a good understanding of the forces to which the astronauts will be subjected. In turn, this understanding allows us to set up a detailed astronaut training program; the astronaut will be subjected to the proper accelerations, for the proper duration of time during training. The loads during launch and re-entry are reasonably high, but will not put the occupants in unnecessary danger. Figure 7 shows the acceleration magnitudes during the flight. The spacecraft reaches accelerations of 3.2g during launch and a high of 4.9g during the re-entry phase.

The maximum velocity reached by the capsule is 1140m/s (Mach 3.6), which occurs during the early re-entry phase. Similar speeds are reached during the ascent. Velocity analysis also shows that, as the capsule passes through the re-entry phase, it continues to slow down. It drops below mach 1 at 16km altitude and reaches a terminal velocity regime at an altitude of 14km. At this stage, we can safely deploy parachutes without special need for additional drogue or stabilization chutes. Also, the velocities are low enough for the pilot to attempt an evacuation in case of parachute-deployment failure. Figure 8 shows the full flight velocity profile.

The trajectory simulator can also be used to determine different mission outcomes based on varying performance characteristics of the launch vehicle. One such analysis looked at the final altitude reached by the rocket based on various vertical launch angles. The rocket will be launched from below a large balloon, suspended in place by a long tether cable, and the initial launch angle can be varied. In order to clear the balloon, either the angle of the rocket must be large (angle is measured from vertical) or the tether cable must be long. It is important to reduce both quantities as much as possible, while still reaching a minimum desired altitude. To allow sufficient room for error, we chose to make our minimum target altitude 110km, even though X Prize rules require only 100km.

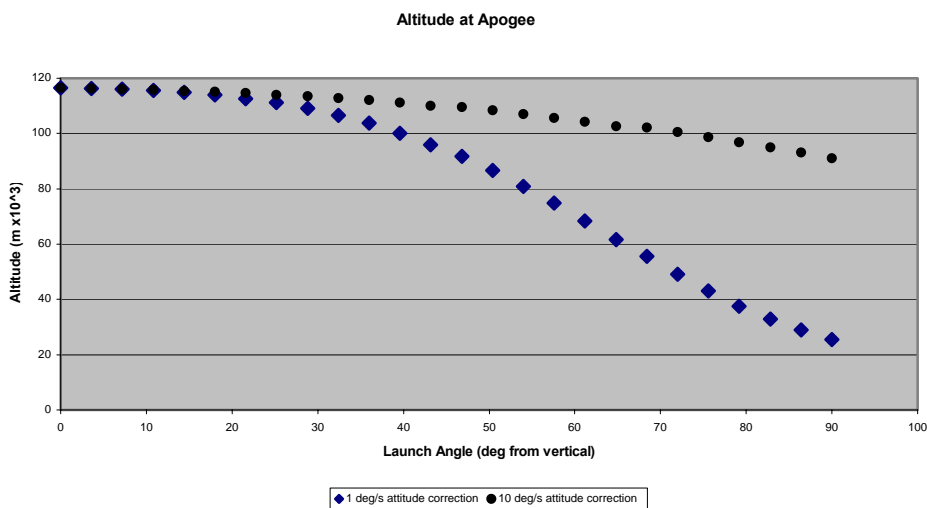


Figure 9. Altitude vs. Launch Angle

We calculated a separate trajectory for launch angles between 0 and 90 degrees off vertical, and using two different angle correction rates, 1 deg/s and 10 deg/s. Once the simulator determines that the balloon will be safely cleared, the rocket starts to correct itself to vertical flight. Figure 9 shows the different altitude outcomes for the two angle correction rates. In fact, if a 1 deg/s correction rate is used, the launch angle can not exceed 28 degrees. If a 10 deg/s correction rate is used, the launch angle can be as large as 45 degrees while reaching the same altitude.

Another important issue to consider is the rocket's downrange flight path. Predicting the flight path in detail is crucial to assessing possible landing locations, recovery, and range safety. We have performed flight trajectories for both anticipated conditions, as well as emergency situations. For a typical flight, the rocket travels mainly in a vertical direction. This means that the largest effect on the downrange flight path is the winds. The winds have the largest influence on the balloon's trajectory, as it spends the longest amount of time in the air. Figure 10 shows the ground tracks of both the balloon and the rocket, plotted over a map of our launch area. The wind data used for this particular simulation was measured on July 25th, 2002, and it accurately represents the conditions for an above average windy day. In this scenario, the overall ground path is approximately 90 km in length. On the day of launch, we will calculate this data based on current atmospheric and wind conditions, and will use it to send ground recovery crews to the anticipated landing zone prior to launch. For proper range safety precautions, we must also consider the worst possible range-safety scenario. To this end, simulations were performed to determine the rocket's maximum possible range. These simulations involved running various trajectories, at a wide range of launch angles. We initiated the launch simulations at our regular launch altitude of 24.4km. In order to



Figure 10. Flight Profile Map from the Launch Site in Saskatchewan (Kindersley)

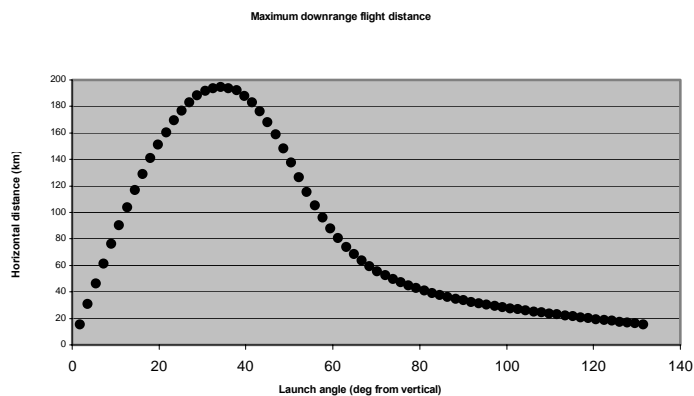


Figure 11. Downrange flight distance vs. launch angle

assume a worst case scenario, we did not correct to vertical flight, and the rocket continued to fire in its pre-determined direction until engine burn-out. There are of course numerous safety systems in place to prevent such an occurrence, but we felt it was useful to know the extent of the vehicle's performance envelope. The data is shown in Figure 11, with a maximum downrange flight distance of 195km, coinciding with a launch angle of 34 degrees from vertical. We did not factor winds into this simulation, as they vary greatly from day to day, but they would have an additional effect on the downrange distance.

3.2 Aeroheating Analysis and External Aerodynamics

Various two-dimensional (2D) and three-dimensional (3D) computational fluid dynamics (CFD) studies were performed in support of multiple design iterations of the rocket block (RB) and of the re-entry capsule (RC). These studies included various spherical, oval, conical RB shapes, several ballute configurations and spherical RC shapes. All studies were performed using CFD-FASTRAN [8] and CFD-ACE+ [9] software packages developed by CFDRC (Huntsville, AL). All analysis were performed for various time positions on the trajectory, i.e. for frozen flow conditions, and covered the range between 100 m/s to 1150 m/s. CFD-FASTRAN is best for supersonic shock wave flow conditions, while CFD-ACE+ is extremely valuable for coupled fluid-solid and fluid & structure flow and heat transfer simulations. Both codes can utilize structured, unstructured and hybrid grids as shown in Fig. 12(a,b). Detailed aerodynamic analyses allowed us to estimate forces and momentums on all components of the RB and corresponding overall C_L and C_D coefficients. These coefficients were in turn used to narrow down mission trajectory uncertainties. Our ability to perform virtual aerodynamic test tube and shock tube tests allowed us to cut a significant amount of time and development costs.

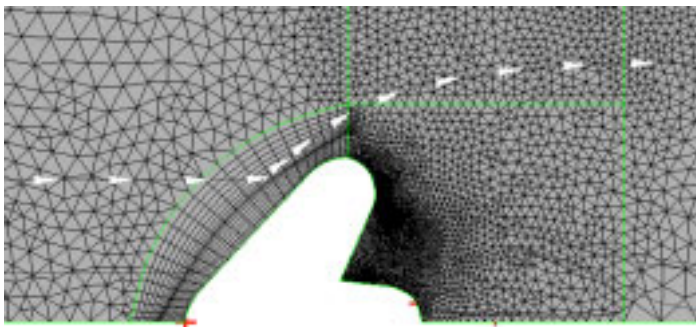


Figure 12a. Hybrid grid around re-entry vehicle and ballute

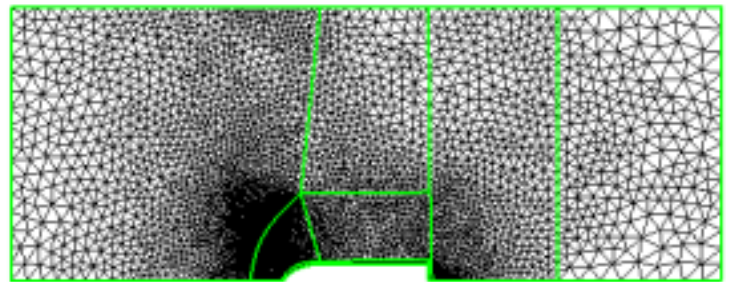


Figure 12b. Hybrid grid around bullet-shaped rocket block

3.2.1 External Heating

External heating analysis [11-13] presented one of the most critical parts of our mission research efforts. External heat flux and equilibrium wall temperature explicitly define the possible range of trajectory scenarios and limit maximum allowable flight altitudes (higher altitude – larger thermal loads). Trajectory integration (described in Sect 3.1) was coupled with Mach number and stagnation temperature/pressure estimation and was followed by compressible Navier-Stokes CFD analysis. We established that peak flow temperatures T_{max} do not exceed 389 deg.C for 100km peak altitude and can be contained below 500 deg. C for apogee range of 100 to 110 km.

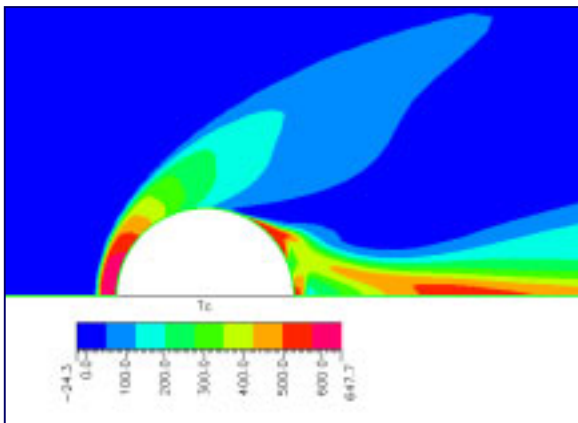


Figure 12c. Temperature Distribution

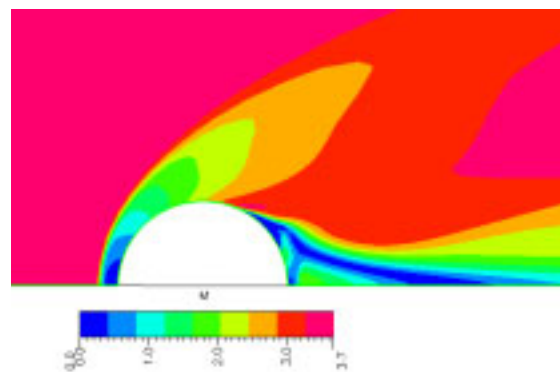


Figure 12d. Mach number (velocity) distribution

From the material standpoint it is desirable to limit maximum flow temperatures below 400 deg.C; with 420 deg. C being the melting temperature for aluminum alloys and 350 deg C for Kevlar composite. Thus the safest thermal entry ‘corridor’ is between 100 to 105 km for the apogee. It is evident that with judicious trajectory management and control it is possible to satisfy X-prize requirements, reach legal outer space (100km), and to maintain structural integrity without an external thermal protection shield. This solution will however minimize safety factor K_s to below 1.1. For a safer flight margin ($K_s=1.5..1.7$) thermal shielding will still be required. In this paper we analyze a 115 km trajectory that corresponds with 66 sec engine burn time. From re-entry trajectory data we extracted several critical points (100 sec, 100 km, apogee, peak stagnation temperature, peak dynamic head, peak velocity and Mach number) and then conducted “frozen flow” CFD analysis with FASTRAN flow solver. Modeling with laminar Navier-Stokes equations was utilized in combination with adiabatic wall boundary condition and isothermal wall boundary conditions (for heat flux estimation).

Temperature distribution and flow velocity (Mach number) maps are demonstrated in Figures 12c and 12d. Flow temperature distribution around the RC is also shown on Figure 17. These results correspond with peak stagnation temperature conditions during the re-entry phase. Stagnation pressure and bow shock wave that corresponds to these conditions are shown in Figure 13 (a,b). Maximum stagnation temperature $T=647$ deg. C (Figs. 12c,17) was obtained from CFD computations for $V=1150$ m/s, altitude of 42.5 km, peak pressure of 47kPa and maximum heat flux of 74 kW/m² (for isothermal wall temperature).

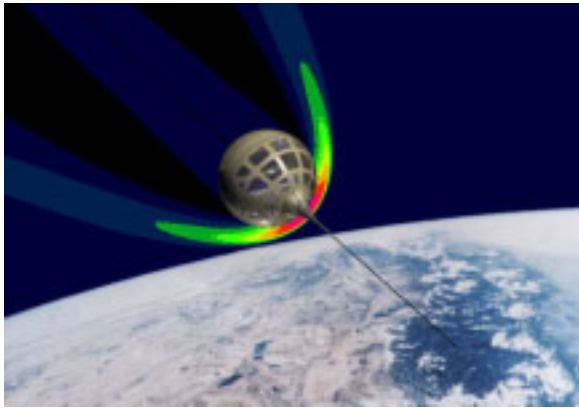


Figure 13a. Shock wave at the re-entry

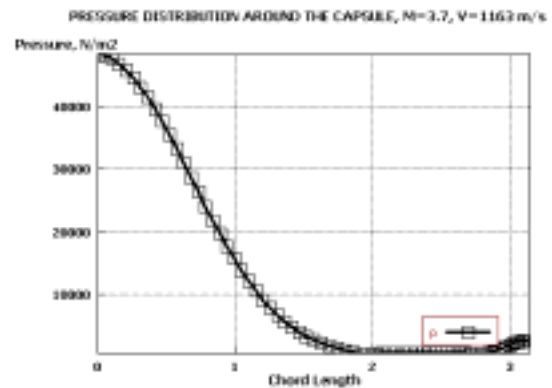


Figure 13b. Pressure distribution around the capsule

3.2.2 Internal flow and Temperature in the RC

CFD analyses were utilized to study temperature rise inside the re-entry capsule. We assumed possible range of wall temperatures between 30 deg. C to 90 deg C and monitored transient free convection internal flow and resulting temperature distributions for 250 sec. Self-sustained averaging of temperature is evident (see Fig. 14a, $t=125$ sec), with top of the vehicle being the hottest and with the zone occupied by the astronauts being the coldest. Results indicate that forced mixing may not be required. Heat accumulates in the upper zone and propagates downwards. On Fig. 14b we demonstrate rise in volume averaged gas temperature for trajectory described in Sect. 3.1. Note that temperature gain can reach between 20 to 25 degrees.

3.2.3 CFD of RC Moving Body Dynamics

For re-entry analysis it is very important to estimate dynamics of the RC motion around its center of the mass. Dynamics of oscillatory movement will be defined by damping forces, which are due to RC lateral transition in the impinging flow and due to RCS. In order to quantify forces and momentums we studied pressure fields around the vehicle due to body rotation (using CFD-ACE+) and due to prescribed motion (using CHIMERA grid technology of CFD-FASTRAN). Forces were extracted and tabulated as a function of velocity, approximations were passed to dynamic motion analysis software (sect 3.6). Example of such analysis is shown on Figure 13c. We can find that pressure symmetry is broken, with pressure higher on the left side and lower on the right. Resulting force is directed from left to right and is responsible for damping capsule vibrations.

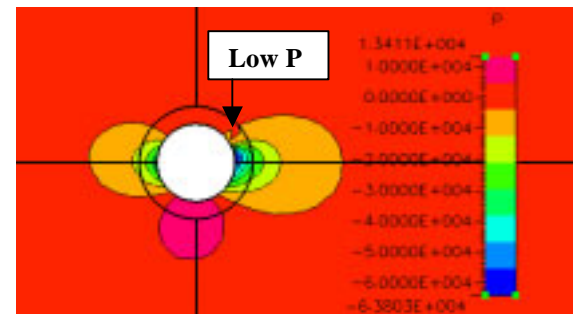


Figure 13c. Pressure field around counterclockwise rotating RC in the impinging subsonic flow (150m/s)

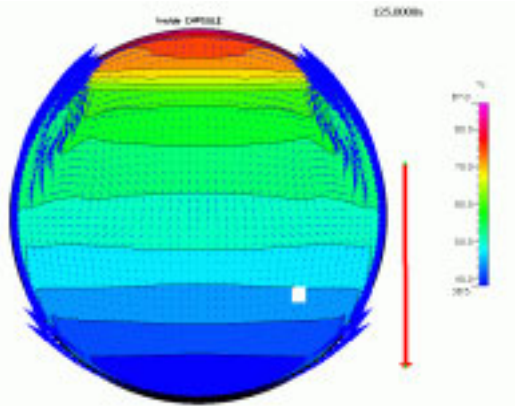


Figure 14a. Temperature Field inside the capsule (125 sec)

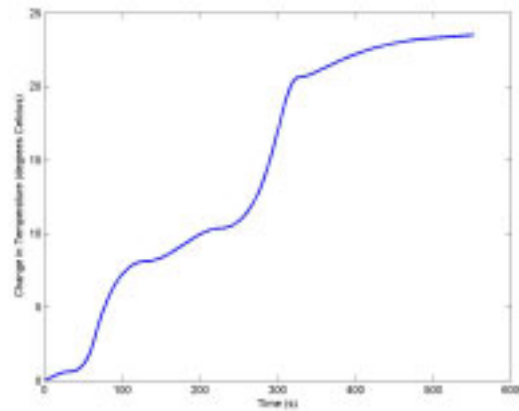


Figure 14b. Time history of mass averaged temperature

3.3 Thermal Protection System Evaluation Analysis

One of the critical safety systems onboard the da Vinci spacecraft is the Thermal Protection System (TPS). A TPS design is needed for both the capsule and propulsion sections. A preliminary analysis of the TPS helped us determine the appropriate material(s) and configuration for the TPS. With a sub-orbital target altitude of 100 km, the spacecraft will re-enter the earth's atmosphere under much lower thermal and pressure loads than a full re-entry from orbit (such as what the space shuttle experiences). Using CFD analysis, we predict a maximum thermal load, at the stagnation point on the re-entering capsule's surface, of 921.09 K [647.94 °C]. For details, see Figure 15. The general thermal load experienced by the capsule (as well as the propulsion section) goes through a cold-to-hot-to-cold cycle.

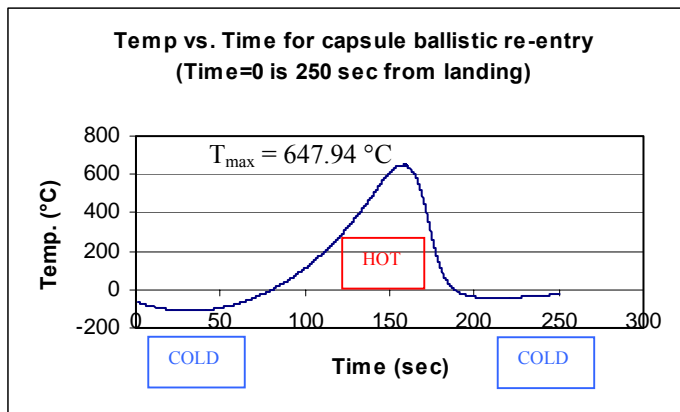


Figure 15. Temperature Profile from the capsule ballistic re-entry simulation

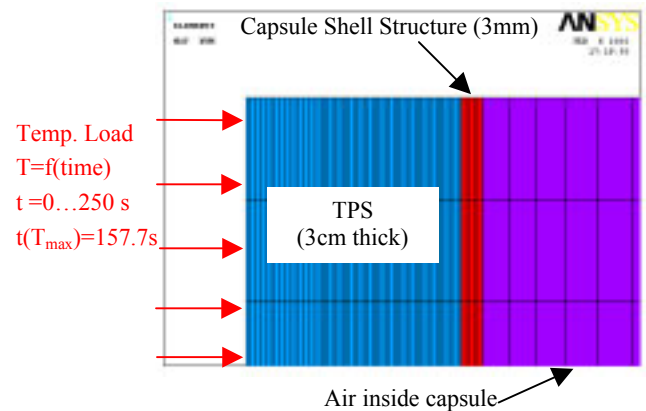


Figure 16. Finite Element model in Ansys. (top left corner of 2-D block)

We researched TPS materials in texts, reports, company websites, and online databases such as NASA Ames Research Center's Thermal Protection Systems Expert and Material Properties Database³. We generated a list of the materials that matched our load characteristics (a maximum temperature of 921.09 °K [647.94 °C] and an aerodynamic flux of 75,000 MW/m²). The list of selected materials is shown in Table 1. We then tabulated and compared the thermal diffusivity of the various materials to get an initial indication of how well each material would perform in the subsequent FEA modeling.

Using Ansys Multiphysics FEA software [10], 2-D finite element block models (shown in Figure 16) were constructed as the basis of a comparative thermal heat wave propagation analysis. Several models were also constructed to facilitate a layered TPS structure, enabling us to determine the efficacy of combining different materials together in various configurations. The initial temperature of

³ <http://tpsx.arc.nasa.gov/tpsx-web.shtml>

the blocks was set to 300 °K [27°C] and the model was analysed over a total trajectory time of 250 seconds, starting at apogee. This is a sufficient time span to fully cover the re-entry phase of the flight. We then compared the heat wave at various times in the capsule trajectory (50s, 100s, 150s, 200s, and 250s). Selected reference points, at various depths within the TPS were also compared. The points—measured from the load bearing side of the block—were set at 0.267cm, 0.533cm, 1.0cm, 1.5cm, 2.0cm, 3.0cm, and 3.3cm (inside surface of the capsule shell).

A 2-D half circle finite element model was created to represent a cross-section of the spherical capsule. This was used to evaluate variation in the heat wave propagation along the circumference of the capsule. As the 2-D block comparison used the maximum transient thermal load from the stagnation point, the actual load along the circumference of the capsule is varied; up to 17 % lower in certain sections (largest temperature difference being 150 degrees). Figure 17 shows the skin temperature distribution that was used to approximate a temperature profile over the perimeter of the full capsule cross-section shown in Figure 18.

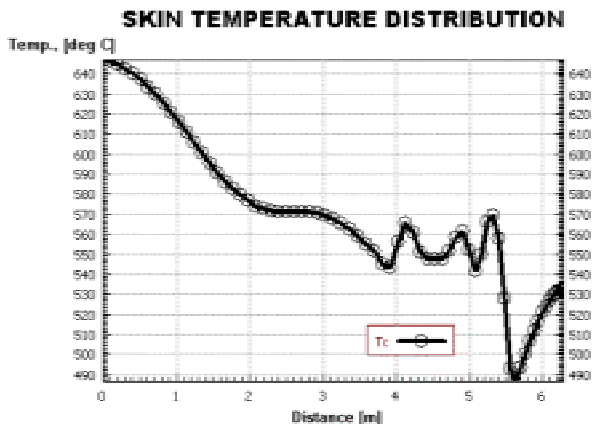


Figure 17. Skin Temperature Distribution along circumference of capsule.

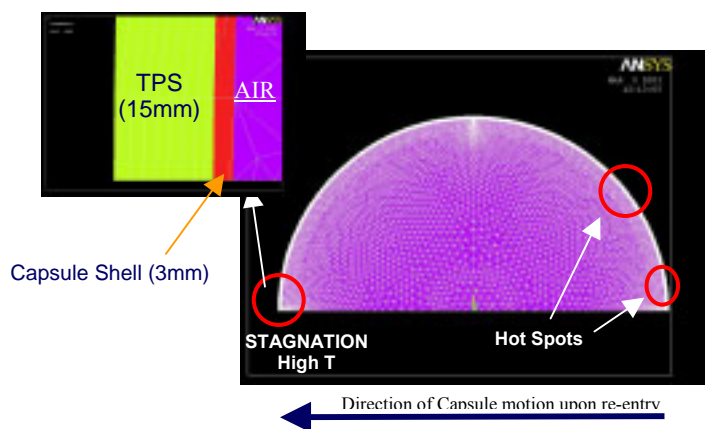


Figure 18. Capsule cross-section finite element model

Material	Manufacturer	ρ [Kg/m ³]	λ [W/m-K]	C_p [J/Kg-K]	α [m ² /s]
Acusil II	Aerotherm	260	0.077	922	3.212E-07
Norcoat 4011	EADS	900	0.15	750	2.222E-07
Norcoat Liege	EADS	470	0.03	750	8.511E-08
Aleastrasil	EADS	1650	0.7	750	5.657E-07
Prosil	EADS	600	0.1	750	2.222E-07
Nextel 312	3M	785.5	0.146	1046.6	1.776E-07
Nextel 440	3M	910.5	0.15	1130.4	1.457E-07
LTC-HSA	Unifrax	192.22	0.07499	1151	3.389E-07

Table 1. Material Property Table

3.3.1 Theory

Thermal diffusivity is the main thermophysical property we are concerned with when selecting materials for our TPS requirements. It is the ratio of a materials thermal conductivity to its heat capacity and it determines the speed by which heat propagates through the material by conduction as its temperature changes with time. The higher the thermal diffusivity, the quicker response to the thermal environment and the faster the heat wave propagates. The thermal diffusivities of the candidate materials are shown in Table 1. Thermal diffusivity (α) is defined as equal to $\lambda/(\rho C_p)$, where λ = thermal conductivity [W/m-K]; ρ = density [kg/m³]; C_p = specific heat [J/kg-K].

3.3.2 Results

The heat wave results at the different trajectory times for the 2-D blocks clearly show that the Nextel 312 & 440 and Norcoat Liege materials responded the slowest to the changing thermal load and were the best in limiting the propagation of the heat wave through the TPS. Nextel 440 was the most efficient thermal barrier. Its performance was closely followed by Nextel 312 since they have very similar thermal properties and Norcoat Liege rounded out the top three.

At 50 seconds into the trajectory within the cold phase of the thermal load the Nextel materials (312 & 440) had no significant temperature drop past 5mm into the material. Norcoat Liege—at 5.33mm—had a temperature drop to 288 °K [14.85°C]. Whereas Aleastrasil saw a temperature drop to 240 °K [-33.15°C] at the same point and time.

The maximum temperature in the thermal load is seen at 157.7 seconds into the trajectory. The plot at 200 seconds (shown in Figure 19) demonstrates the heat wave that resulted from the high temperature portion of the thermal load. Both the Nextel and Norcoat Liege materials had no temperature change past a depth of 1.0 cm. All the other materials had significant rises in temperature past the 1.0 cm point. The heat wave in Aleastrasil propagated to a depth of 2.5cm.

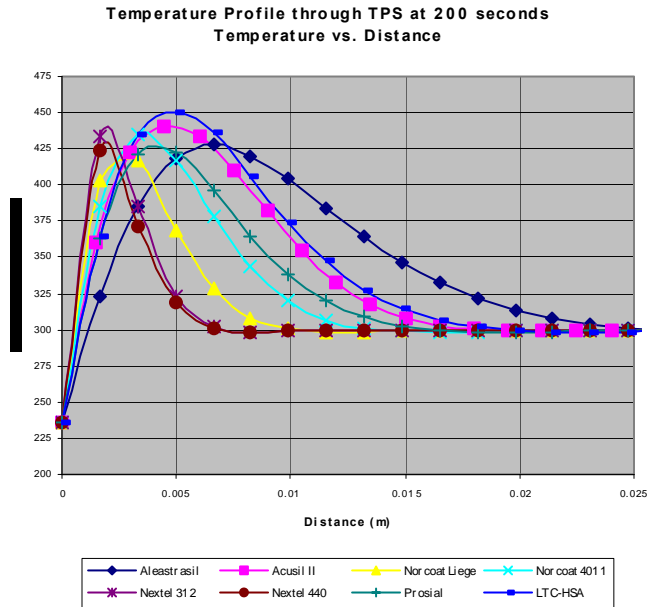


Figure 19. TPS Temperature Profile at 200 s.

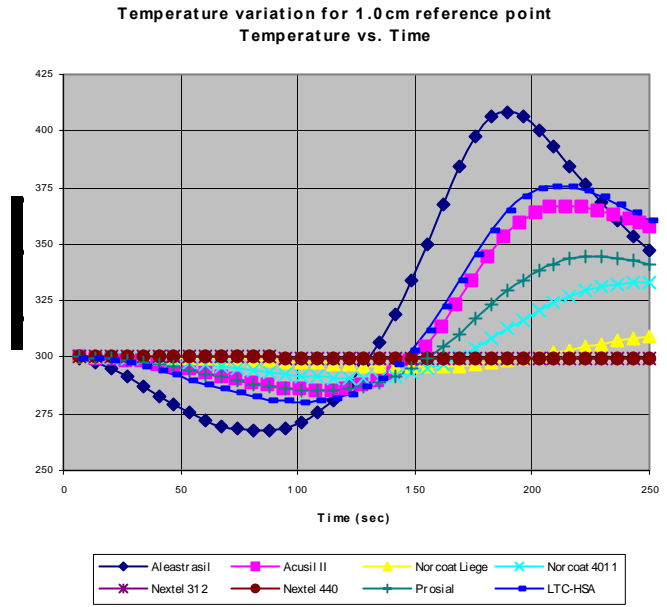


Figure 20. Variation in Temperature for 1.0 cm reference point in TPS.

All of the reference point plots showed that there was the least temperature change with Nextel 440, Nextel 312, and Norcoat Liege (in order of increasing temperature change). Figure 20 shows the variation in temperature at a depth of 1.0 cm throughout the trajectory for the various materials. Aleastrasil had the highest rise in temperature, reaching 408.5 °K [135°C]. A summary of the maximum temperatures at the various reference points is shown in Table 2. From this table it is clear to see the depth of thermal propagation within each material. The thermal wave in Aleastrasil propagated all the way to the outside of the capsule shell with only a slight one degree increase from the initial condition of 300 °K [27°C]. The Norcoat and Nextel materials had no temperature change past a depth of 2.0 cm, while the Nextel materials prevented any temperature change past the 1.0 cm point. At a depth of 1.5 cm all of the materials had temperatures between 300 °K [27 °C] and 330.7 °K [57.55 °C], except for Aleastrasil which had the highest maximum temperature of 350.6.

Material	0.267cm	0.533cm	1cm	1.5cm	2cm	3cm	3.3cm
Aleastrasil	690.1	542.9	408.5	350.6	326.1	301.0	300.9
Acusil II	639.7	485.5	367.0	324.8	304.9	300.0	300.0
Norcoat Liege	484.1	360.0	309.5	300.0	300.0	300.0	300.0
Norcoat 4011	574.7	415.7	333.2	305.5	300.0	300.0	300.0
Nextel 312	424.0	330.1	300.0	300.0	300.0	300.0	300.0
Nextel 440	405.8	325.0	300.0	300.0	300.0	300.0	300.0
Prosilal	594.8	439.0	344.2	313.8	301.6	300.0	300.0
LTC-HSA	655.4	500.6	375.5	330.7	308.6	300.0	300.0

Table 2. Summary Table of maximum temperatures at reference points

Material	Thickness [m]	Max temp [K]	Density [Kg/m3]	Mass [Kg]
Acusil II	0.015	324	260	47.8
Norcoat 4011	0.01	333	900	109.7
Norcoat Liege	0.0075	328	470	42.9
Aleastrasil	0.02	326	1650	406.5
Prosilal	0.0125	330	600	91.7
Nextel 312	0.00533	330	785.5	50.8
Nextel 440	0.00533	325	910.5	58.9
LTC-HSA	0.015	330	192.22	35.3

Table 3. Material Mass Comparison Table

The preliminary layered TPS models consisted of variations of Nextel 440 and LTC-HSA. Table 4 shows a summary of the different layered models, the resulting maximum temperature seen at the outside of the shell (target temperature), and the configuration's mass breakdown. For comparison, the single layer Nextel 440 and LTC-HSA are also included. The different configurations yielded very similar outer shell temperatures in the area of 308 °K [34.85°C] with a largest variance of only 7.3 degrees. Their corresponding masses were also similar and averaged out to 44.52 kg with a largest variance of 5.7 kg. The best results were seen with a 1 mm Nextel layer followed by a 13 mm LTC-HSA layer (1N-13L). This configuration resulted in the lowest maximum outer shell temperature of 304.3 °K [31.15°C] and the lowest total mass of 41.6 kg.

Layer Configuration	Tmax (K) Capsule Shell	Mass [kg]		
		Nextel 440	LTC-HSA	Total
15L	330	n/a	35.3	35.3
5.33N	325	58.9	n/a	58.9
3N-6L	311.6	33.1	14.1	47.2
2N-9L	308.3	22.0	21.2	43.2
1N-13L	304.3	11.0	30.6	41.6
1N-9L-1N	308.5	22.2	21.1	43.3
1N-2L-1N-2L-1N-2L	308.8	33.2	14.1	47.3

Configuration Definitions:

N = Nextel 440
 L = LTC-HSA
 Number represents layer thickness (mm)
 Ex: 2N = 2 mm layer of Nextel 440
 Layers are read from left to right (outer TPS to inner TPS)

Table 4. Maximum Temperature on outer capsule shell with different layered TPS configurations and the resulting mass.

For the cross-section model of the capsule sphere, the coldest spot along the circumference was as at a chord length of 1.76 m. A target outer capsule shell temperature was selected at 320 °K [46.85 C] in order to compare the minimum TPS thickness required for that target temperature at the hottest spot (stagnation point) and the coldest spot (at 1.76 m chord length). The 250 s trajectory time was used as this was the time at which there was the greatest thermal penetration. As shown in Figure 21, at the stagnation point the minimum thickness was 9.4 mm while at the 1.76 m chord length point, the minimum thickness was 10.6 mm. This results in a total difference of 1.2 mm.

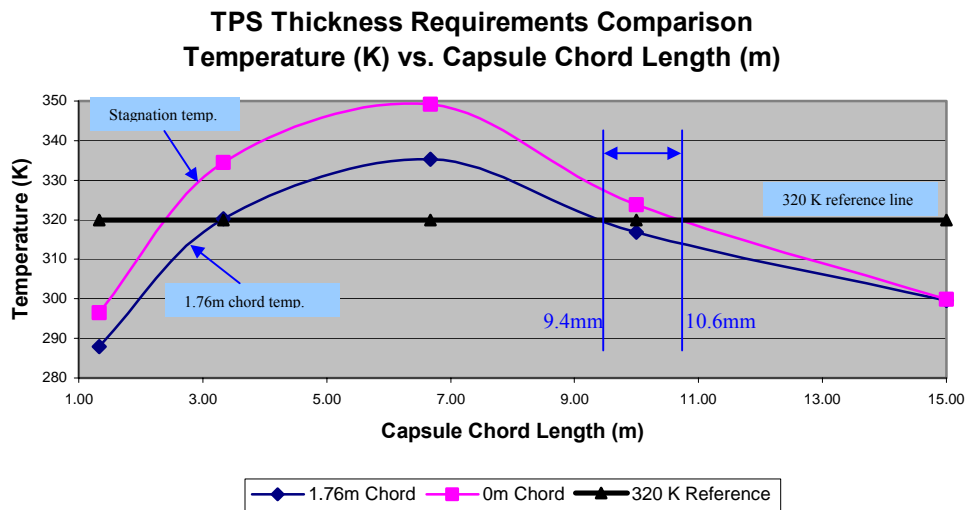


Figure 21. Comparison of Cold and Hot spot thermal propagation at 250s

3.3.3 Discussion

The best results were achieved with those materials that had the lowest thermal diffusivity; as to be expected. Comparing materials by thermal conductivity alone is not sufficient. The LTC-HSA (Low Thermal Conductivity – High Surface Area) material had the second lowest thermal conductivity but did not provide an adequate thermal barrier relative to the other materials. This was due to its low density which contributed to a higher thermal diffusivity.

The 2-D block results obtained enabled us to gauge how much (thickness of TPS) of a certain material would be necessary in order to limit significant thermal propagation from our predicted loads. Nextel (312 & 440) and Norcoat Liege were the least sensitive to their thermal environment and provided the best thermal protection with the least thickness. At a depth of 1.0 cm all three materials would sufficiently provide adequate thermal protection. However, there are other equally important factors that must be considered such as the total mass of the system. Table 3 shows a comparison of the required thickness—and resulting mass—of each material in order for the target temperature of the outside of the capsule shell not to exceed 333 °K [59.85°C]. The selection of a final structural capsule shell material will have an impact on the TPS design by altering the target maximum temperature for the outside of the shell. A material like Aluminum will be much more sensitive to the thermal environment than Kevlar and would thus lower the target maximum temperature that must be designed for; this could in turn increase the TPS thickness. From Table 3 we can see that the best materials when factoring in strict mass constraints are Norcoat Liege, Acusil II, and LTC-HSA with masses of 42.9 kg, 47.8 kg, 35.3 kg, respectively. Among those materials Norcoat Liege was only 7.5mm thick, and Acusil II and LTC-HSA were both 1.5cm thick. Nextel 312 & 440 at thicknesses of 5.33mm and with masses of 50.8 kg and 58.9 kg respectively are also substantially lower than the rest of the other materials.

Even though LTC-HSA had the lowest mass of only 35.3 kg, its ablative properties would not allow it be exposed to the outer environment upon re-entry and therefore any TPS with LTC-HSA would need to have an outer layer. One such configuration could be with Nextel 440. The preliminary results show that there is a mass savings when combining these materials. The single 5.33 mm layer Nextel 440 TPS had a mass of 58.9 kg with an outer shell maximum temperature of 325 °K [51.85°]. Where as the 1N-13L configuration had an outer shell maximum temperature of only 304.3 °K [31.15°C] and only weighed 41.6 kg. A mass savings of 17.3 kg, which is fairly substantial when we take into account the capsule's strict mass constraints. The outer shell maximum temperature was also lower by 20.7 degrees. Decreasing the LTC-HSA layer thickness to allow for a greater outer shell maximum temperature would decrease the mass even further. The rest of the layered models also showed similar reductions in overall mass. The Nextel-LTC-HSA layered approach yields better results over single layer models with the same materials. Further layered trials will be conducted to evaluate this approach.

Another method to reduce TPS mass would be to vary the thickness of the TPS along the circumference of the spherical capsule. The results of the cross-section model showed that the maximum difference in the minimum TPS thickness between the hottest and coldest points would be 1.2 mm. This value is approximately 10% of the TPS thickness at each point. This result gives us minimal mass savings when one considers that the 1.2 mm thickness difference is only at one small section of the capsule. It would be more beneficial to have an extra safety factor in certain sections, and simplify our manufacturing process by applying a uniform TPS thickness over the entire surface.

3.3.4 Validation

In order to confirm the accuracy of our Ansys results, two comparisons were performed using the explicit finite-difference method. For the first comparison, an example was used from a heat transfer text⁴ of a copper block with a constant heat flux load applied to one side. The text provided various solutions including an exact solution. An Ansys result of the same problem was compared to the finite difference method programmed with Maple software, and the exact solution. It was found to have very good agreement between the methods; with the largest variation being 0.43%. The second comparison was of 1-D heat conduction through a 3cm block of Acusil II with a constant temperature load applied to one side. The variation between the Ansys result and the explicit finite-difference model was 0.16%. These validation results raise our confidence level in the results that we are getting from Ansys. Future validation work will also be performed through experimental results.

3.3.5 Summary

The CFD analysis gave our predicted thermal loads, which then led to a variety of candidate materials that could be used for the capsule TPS. Using Ansys, preliminary comparative analysis of the various materials resulted in the selection of Nextel 312, Nextel 440, and Norcoat Liege as the best materials for limiting the thermal propagation with the least TPS thickness. Norcoat Liege and LTC-HSA were overall the best when factoring in mass requirements. Norcoat Liege would be only 7.5 mm thick, with a mass of only 42.9 kg, while LTC-HSA would be 1.5 cm thick with a mass of 35.3 kg; not taking into account other TPS design factors such as ablative properties. A layered configuration of Nextel and LTC-HSA provided a substantial mass savings versus single layer TPS with the same materials. Our load data resulted in a maximum varied TPS minimum thickness of 1.2 mm between the coldest and hottest sections and did not pose a substantial reduction in mass. For increased confidence in our Ansys results validation tests were performed using other examples and programs, and at worst, the largest deviation was found to be only 0.43%.

⁴ DeWitt D. P., Incropera F.P., Fundamentals of Heat and Mass Transfer, 4th edition. John Wiley & Sons, New York 1996; page 257 Example 5.8.

3.3.6 Future Considerations

Other design factors of importance will also be factored in; such as ablative properties, radiation, application, operability etc. Gathering a wider range of thermal properties for the materials will allow for more accurate results (i.e. C_p and λ with respect to temperature). An appropriate target temperature for the outside of the capsule shell will be determined to finalize a TPS selection. The balloon ascent temperature profile will be incorporated into the modeling in order to determine the extent of capsule cooling under the parachute and the effect on the internal capsule temperature. Three dimensional finite element models will be created from CAD files in order to more accurately determine the heating of various components, as well as any resulting thermal stresses. Once a TPS selection is made we will engage in experimental testing in order to validate all of our results. As well, we will begin designing the windows for the capsule and the TPS for the propulsion section.

3.4 Balloon Launch Implications

The balloon launch, while providing a great advantage by allowing for a high altitude launch, also poses some unique challenges. Figure 22 shows a typical balloon ascent profile. Note the reduction in rise rate while passing through the tropopause. The time required to reach altitude is quite long, to the order of 85-95 minutes. During this time the occupants of the spacecraft must be in a comfortable environment. At such high altitudes, this requires a supply of oxygen, as well as maintaining an acceptable temperature within the cabin. The mass of the equipment required for this task is too great to be carried

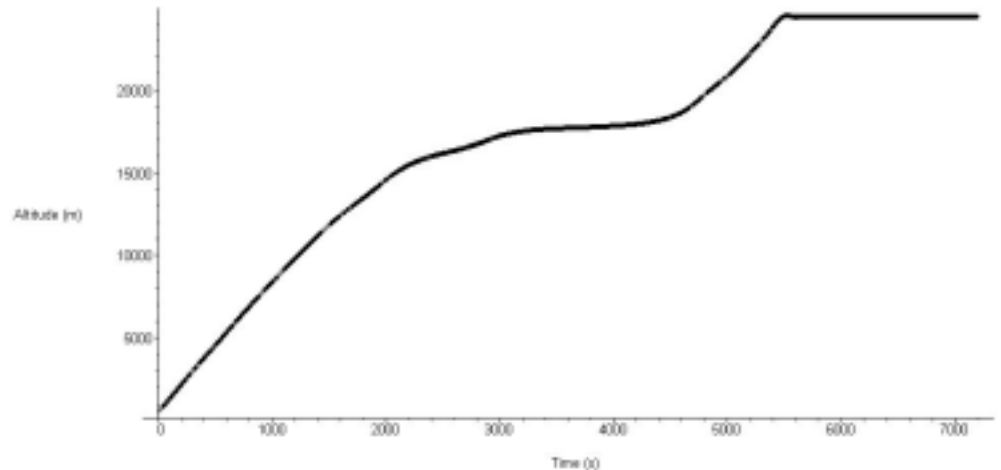


Figure 22. Typical balloon ascent profile

within the rocket itself. This equipment will be carried aboard the Inter-Stage Adapter (ISA), a housing located along the tether between the balloon and the spacecraft. The life support system on board the spacecraft will be connected to the ISA with an umbilical cord, carrying oxygen and electrical power. Low temperatures at altitude pose another serious threat. As our spacecraft will only be in space for several minutes, there is no need for an on-board heating system. Keeping warm for the duration of the balloon ascent can therefore become a serious issue. Studies are currently under way to analyze various different options for capsule heating. Heat retention through the use of insulating materials is the preferred option, and analysis is under way to determine the exact thickness (and therefore mass) of material required. Also, a significant amount of heat can be gained through the sun's radiation entering through the window, and heating the outside of the capsule. This can only be counted on during the day however, and this source of heat might not be available in the very early morning hours. Balloon launch will most likely occur in the early morning, as the surface winds are most benign at this time. A small electric heater may also be provided within the crew capsule for the ascent phase, but this would be a last resort option.

The balloon trajectory after rocket launch is also of great interest. The balloon will suddenly experience a rapid rise due to the release of a significant portion of the total mass. The balloon is expected to rise up to an altitude of 30km once the rocket is released. This is the maximum ceiling, based on the current 170 000m³ balloon volume, and may not necessarily be reached if balloon descent is immediately initiated by opening all of the He dump valves. The rapid ascent after rocket launch can cause the balloon to over-pressure if He is not dumped fast enough. Models show that a maximum pressure difference of 300 Pa can occur. This is within the strength limits of the skin material, and will not cause a rupture.

Balloon recovery is another critical issue. To qualify for the X Prize, the launch vehicle must be reusable. This includes the balloon. Unfortunately, most high altitude balloons are simply destroyed after use. They are made of extremely thin plastic, and brought down by ripping a big section of the balloon in order to release the gas within. In order to achieve true reusability, our balloon must be fully recoverable. Helium venting will be achieved through vents installed in the balloon cap, and the balloon will return to earth under a large parachute, with a 6m/s impact velocity. The parachute will be attached to the balloon cap, and pre-deployed on top of the balloon. As the balloon begins to descend, the parachute will inflate with minimum stress on the balloon and at a relatively low airspeed, reducing damage to the balloon during descent. The parachute attachment to the cap will help to gently lay out the balloon upon landing. The ISA will land first, and the rest of the balloon will be slowly drawn out downwind by the parachute. A thicker material for the balloon envelope is also being considered, as well as multiple skin layers. It is critical to reduce damage to a minimum.

3.5 Sub-systems - parachute

The spacecraft will be recovered in two components, the crew capsule and propulsion section. The two will fall back to earth separately, and once past the atmospheric re-entry phase, will descend under parachute. In order to minimize impact loads, and still maintain a reasonably sized parachute, a 6m/s landing speed has been chosen. This results in relatively large parachutes for the re-entry vehicles. Parachute diameters will be in the 28m range for both sections of the spacecraft. The main consideration in choosing parachute deployment altitude has been the time remaining to impact (Figure 23). We wanted to make sure that the pilot will have sufficient time to evacuate the capsule in the event of parachute deployment failure. As a further safety precaution, there will be redundant parachute systems on the capsule, and the pilot will have a parachute on his person as well. A deployment altitude of 10km has been chosen, leaving the pilot 20s to determine if there was a failure, and a full minute to evacuate if necessary. At this altitude the air velocity of the capsule is approximately 160m/s.

With the pilot's safety in mind, we are trying to limit the parachute deployment force, such that the capsule will not experience accelerations of more than 4g.

Two different parachute configurations are under investigation. The first is a single, large parachute (with a backup chute), that will take the full load. The second is a three parachute system, where the load is evenly distributed between the parachutes. No backup system would be in place, but the parachutes would be rated such that a safe landing was possible with only two chutes deployed. Such a system has the advantage of immediate deployment of all three parachutes, and a system failure is immediately noticed. With a single chute system, if the first deployment fails, the backup must be deployed afterwards. It effectively takes twice as long to determine if a total system failure has occurred. However, a three parachute configuration runs the risk of entanglement in the deployment phase. Investigation as to the optimal system is still under way.

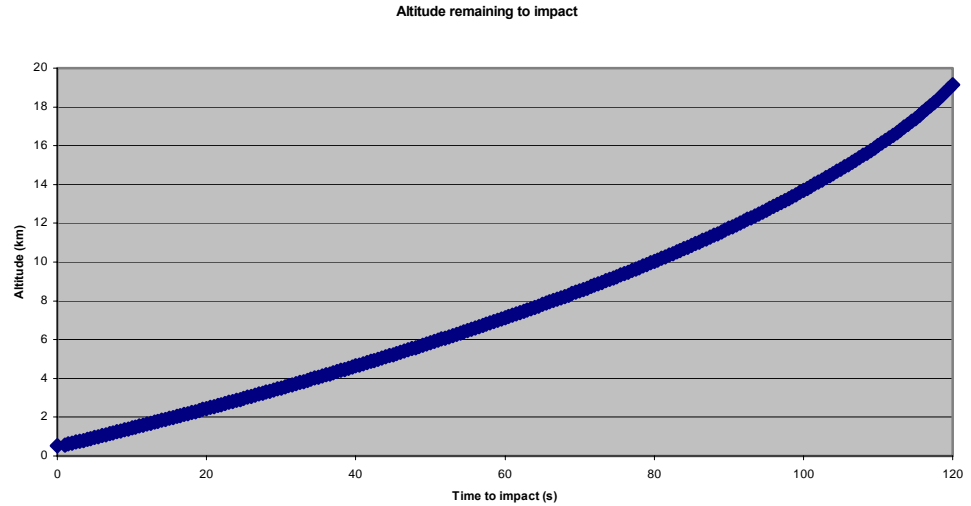


Figure 23. Parachute deployment considerations: Time remaining to impact

Investigation as to the optimal system is still under way.

3.6 Flight Mission Analysis Tools

The da Vinci spacecraft has one main hybrid engine used to propel it forward, and a Reaction Control System (RCS) is used to control the direction of flight. Since there are many flight mission scenarios which need to be analyzed before the real flight occurs, an easy to use tool needed to be developed. The flight mission scenario results are also used to optimize the design of the space craft. These tools will help to ensure that the flight will be safe and successful.

The flight mission analyzer software was developed using MathWorks, Matlab® and Simulink® environment. Matlab integrates mathematical computing, visualization, and a powerful language to provide a flexible environment for technical computing. Simulink is an interactive tool for modeling, simulating, and analyzing dynamic, multidomain systems. It lets you build a block diagram, simulate the system's behavior, evaluate its performance, and refine the design. Simulink integrates seamlessly with Matlab, providing you with immediate access to an extensive range of analysis and design tools.

Matlab is used to create a graphical user interface between the flight mission input parameters and the dynamic simulator, as shown in Figure 24. A list of input parameters which may be modified include: main engine thrust characteristics, space craft geometries and masses, balloon size, desired launch clearance of the balloon, launch height, and parameters which specify when to separate the space craft into two parts, when to deploy parachutes, when to enable air breaks etc.

Once all the parameter values have been specified, pressing the simulate button will launch the spacecraft and all flight data will be recorded. This flight data can be retrieved at any time to analyze all the flight details. Plots are also easily generated to show how the spacecraft flight characteristics changed during the progression of time. A list of flight characteristics which can be plotted include: position, velocity, acceleration, mass, angle of the space craft, aerodynamic forces, temperature, pressure etc. Figure 25 below shows a plot of the spacecraft's orientation with respect to the vertical. The spacecraft started at an initial angle of 15 degrees, and once it had cleared the balloon, the RCS began to fire to correct the angle. At around the 20 second mark, the spacecraft is pointing straight up. From here on, the RCS is fired to correct the space crafts angle due to thrust asymmetries and other disturbances.

The Matlab mission analyzer software also suggests certain parameter values based on other parameters which have already been input. For example, the user must specify the balloon diameter which will be used to lift the space craft, a minimum balloon clearance that you wish to have when avoiding collision with the balloon and the length of the tether used to suspend the space craft below the balloon. Based on these three values, a minimum launch angle is calculated and recommended to the user. This is shown in Figure 26 below.

This software can also be used to predict how accurate the main engine assembly process needs to be to guarantee a successful flight. For instance, when the main engine is perfectly aligned with the space craft, the thrust will be directed in the desired direction. However due to construction or assembly errors, the main engine may not point directly inline with the space craft. The thrust caused by this asymmetric will cause the space craft to pitch in one direction. During the flight, the RCS will expend fuel to try to correct the spacecrafts angle of attack, however there is only a finite amount of RCS fuel to be used. By analyzing the spacecraft flight trajectories [13,14], one can figure what is the maximum engine asymmetry which will still guarantee the space craft to reach 100 Km. This analysis was performed and the plot generated is shown in Figure 27.

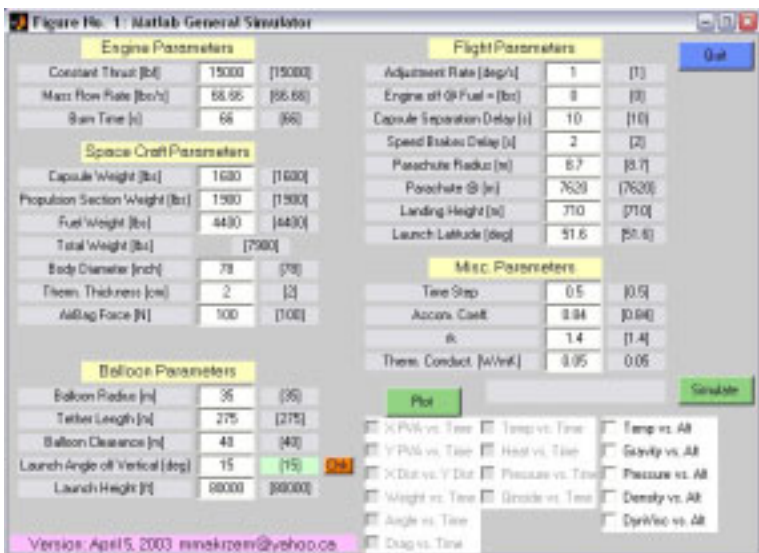


Figure 24. - Matlab Graphical User Interface

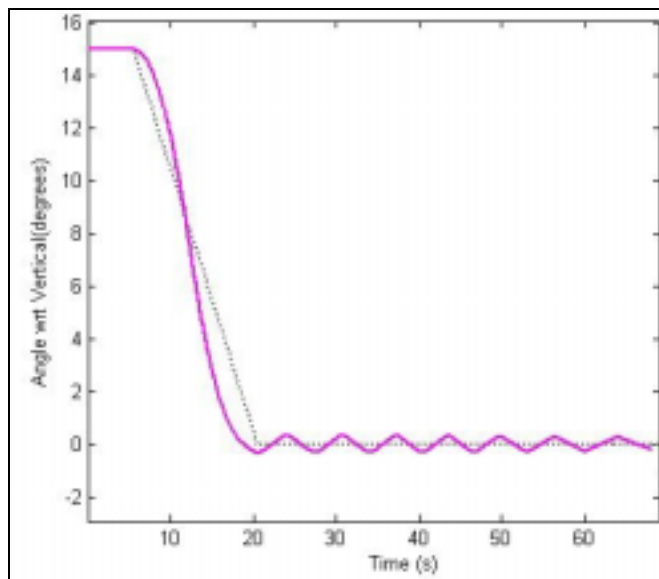


Figure 25. RCS Angle Correction

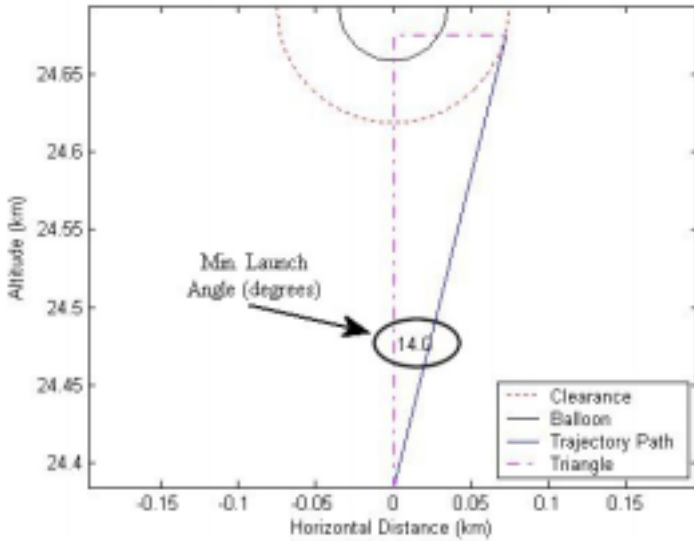


Figure 26. - Minimum Launch Angle

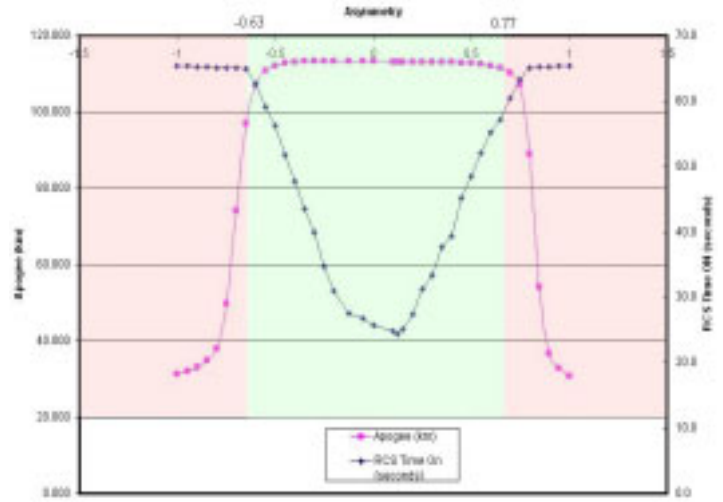


Figure 27. Engine Asymmetry Analysis

On this plot there are two curves. The red curve corresponds to the maximum apogee which the spacecraft reaches. The scale for the apogee height is shown on the left side. The blue curve corresponds to the amount of time that the RCS is on. The scale for the RCS time is shown on the right side. The horizontal scale on the plot represents the amount of asymmetry in degrees of the main engine.

The green band in the middle shows acceptable asymmetries in the main engine to attain an apogee of 100Km. The calculation shows that the main engine must be aligned within -0.63 and +0.77 degrees of the centre line for this particular spacecraft configuration.

Spacecraft dynamics can also be monitored using this software. Since all flight data is recorded during the simulation, a play back of the spacecraft's position and orientation can be very important when doing flight analysis. A mission was created where the RCS system fails to operate and the main engine has an asymmetry equal to 0.8 degrees. From Figure 28 we see that the spacecraft goes into a tumble under these conditions. The spacecraft started at 80,000 feet when the main engines are fired. Almost instantly, the spacecraft begins to point itself downward and tumble end over end. When the capsule separates, it continues to tumble all the way down until it reaches the ground. The software is slowly evolving as more accurate models for physical systems are incorporated. Currently the software only tracks the spacecraft in two dimensions but this is going to be expanded to three dimensions shortly. Also, the second half of the spacecrafts needs to be tracked after separation as well, to ensure that the two pieces have a very low probability of colliding while they are in free fall. Once the simulator is running in 3D, plans are to incorporate a joystick input to the rocket control system, so that manual control of the space craft can be tested. This will allow the pilot to practice and prepare him/her self for the real flight.

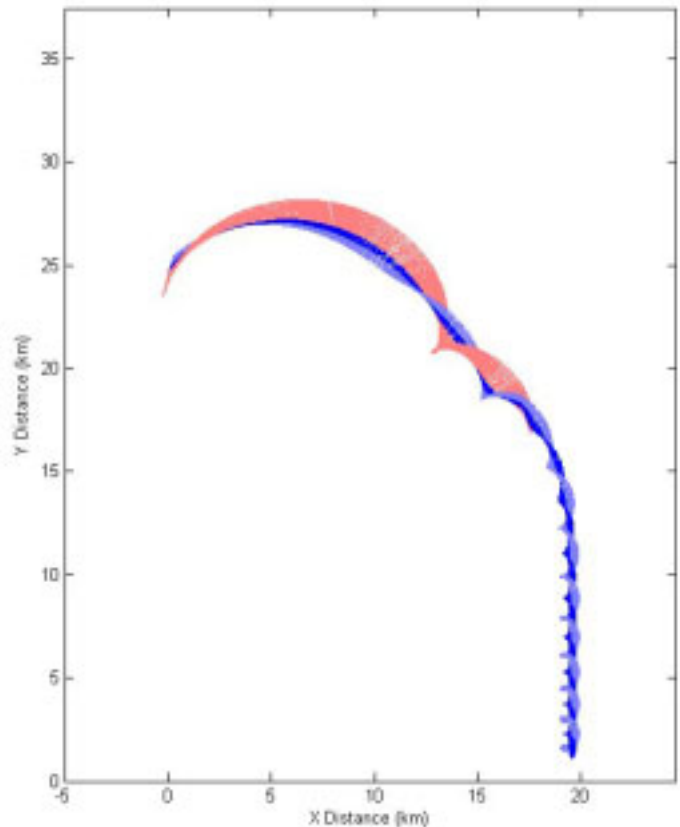


Figure 28. Test Mission Results

3.7 STRESS LOADS – CAPSULE

3.7.1 Introduction

The linear stress analysis for the capsule was performed using Ansys Finite Element Analysis (FEA) software. The geometry was based on 3 mm thick steel spherical capsule shell with an outer diameter of 1980 mm. A Kevlar/Glass material will be studied in the next analysis. The loading cases were given as:

- 1) Case 1: capsule in space with internal pressure 101 Kpa (KN/m²).
- 2) Case 1a: capsule at re-entry with internal pressure 101 Kpa and 50 Kpa external pressure over lower half of capsule.
- 3) Case 2: trajectory, with 101 Kpa internal pressure and 30 Kpa at the top gradually reduced to 3 Kpa at the middle of capsule. Also with a 66800 N (15000 lb) engine thrust force and a 7350 N capsule self weight at the capsule mounting ring.
- 4) Case 3: hard landing with 4 Mpa equivalent static pressure at bottom tip over 100 mm radius area.
- 5) Case 3a: soft landing, with air bag pressure, but this case was not included in this analysis.
- 6) Case 4a: chute deployment using equivalent static force of 126000 N, based on a 0.5s deployment time to simulate the dynamic load. The force was applied at 3 locations, 120 degrees apart on the top of the capsule.
- 7) Case 4b: static hanging with self-weight of 7350 N force.

3.7.2 Model Concept

Before the actual analysis began, four different FEA models were tested in order to select the appropriate model for capsule structure. The first three models were; a plate element (SHELL63), 8-node brick element (SOLID45), and 20-node brick element (SOLID95). These three models had only one element throughout the thickness of the capsule shell. The fourth model tested was with 8-node brick elements and had 3 elements throughout the shell thickness (SOLID45). The above models were tested with a 260 Kpa pressure over the entire outer surface. All the models had the same mesh density. From Table 5, the 8-node brick element with 3 elements through thickness could obtain the best results compared with a theoretical solution. The 8-node brick element with one element through thickness could also get a little bit better results than plate elements. Therefore, 8-node brick elements, with one element or three elements through thickness were used in the analysis. The mesh density was also different for those two types of model. One element type had 1152 elements while three elements type had 41472 elements due to some concentrated forces applied. For case 1 and case 3, one element in thickness was used because of it has less degree of freedom and CPU time. For capsule under load case 1 with only internal and/or external pressures, one element in thickness was good enough to get precise results. For case 3 the hard landing case, the impact pressure was applied near the bottom where very fine mesh already existed, so it was not necessary to use a fine mesh for other places. For cases 2 and 4, a fine mesh was required in the zones of concentrated forces.

The inertia relief concept was used in the analysis to counter-balance all the applied forces/pressure at one constraint point. This could remove the stress concentration near it. This constrained point, either on the capsule top or bottom depending on forces location, was fixed at all six degrees of freedom. All models were created in Global Spherical Coordinate System.

Element type	Stress range (Mpa)	Remarks :
Theoretical solution	42.9	1.98 m diameter sphere with 3 mm (3E-3m) thick steel under uniform external pressure 260 Kpa Theoretical stress = (pressure*diameter)/(4*thickness) 1 Mpa = 1 MN/m ² = 1 N/mm ²
Plate element (shell63)	42.2 ~ 42.7	
Brick element 8 nodes (solid45)	42.2 ~ 43.3	
Brick element 20 nodes (solid95)	42.8 ~ 43.7	
Brick element 8 nodes with 3 elements in thickness (solid45)	42.7 ~ 43.2	

Table 5. Ansys Element Types Comparison

For the hard landing case, the equivalent static load (F) was obtained from the change of momentum during the impact time of 0.1s. That is, $F = (M \Delta V) / t = 75000 \text{ N}$, use 120000 N conservatively.

Then, maximum pressure = $F/A = 4 \text{ Mpa}$

where :

$M = 750 \text{ Kg}$ capsule mass

$\Delta V = 10 \text{ m/sec}$ = change of velocity, from 10 to 0,

Impact time, $t = 0.1 \sim 0.25 \text{ seconds}$, use 0.1 s

$A = \text{impact area of } 100 \text{ mm radius} = 31400 \text{ mm}^2$

The dynamic load for chute deployment is statically assumed as

$$F = (MV_1 - MV_2) / t = 126000 \text{ N}$$

where,

$M = 750 \text{ Kg}$ capsule mass

$V_1 = 90 \text{ m/sec}$, velocity before deployment

$V_2 = 6 \text{ m/sec}$, velocity after deployment

Deployment time $t = 0.5 \text{ sec}$ (generic extreme scenario was considered, chute deployment time typically exceeds 10 sec).

3.7.3 Results

For each load case the deformation plot was checked first to make sure the model was simulated correctly. Then the stress results were listed in Tables 6 and 7. Note that for linear stress analysis we only consider range of von Mises stress below yield point (350 Mpa). Thus, cases 3, 4a,4b represent mechanical failure scenarios.

Loading cases	Max von Mises Stresses (Mpa)
case 1 in space	16.9 (int. pres. 101 Kpa)
case 1a re-entry	18.0 (int. pres. + ext. pres.)
case 2 trajectory	103.8 (pres.+thrust+self wt.)
case 3 hard landing	1148 (pressure 4 Mpa)
case 3a soft landing	--- (pending)
case 4a chute deployment dynamic	8278 (total force 126K N, deployment time 0.5 sec)
case 4b chute deployment static hanging	483 (total force 7350 N)

Table 6. Stress Results

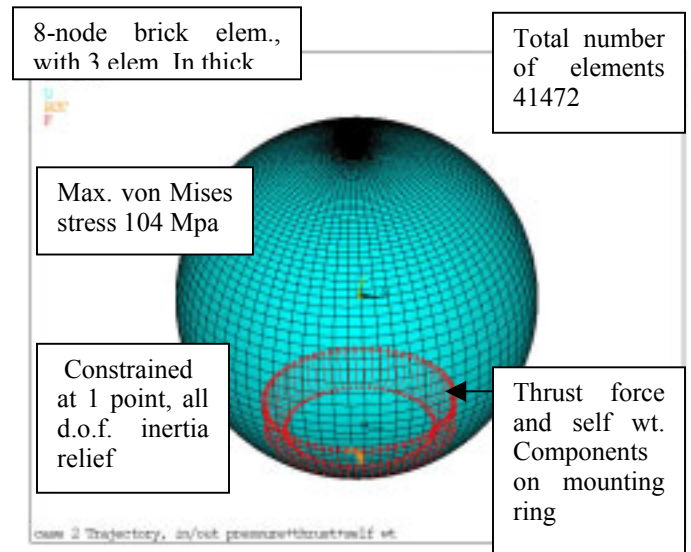


Figure 29. Model of Case 2 - Trajectory with Internal/External Pressure (not shown here) and Thrust force plus Self Weight

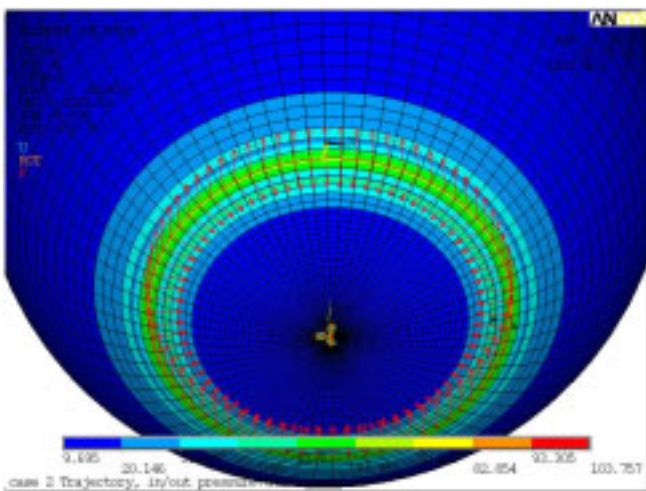


Figure 30. Case 2 Trajectory Stress Results Near Thrust Force Locations, von Mises Stresses

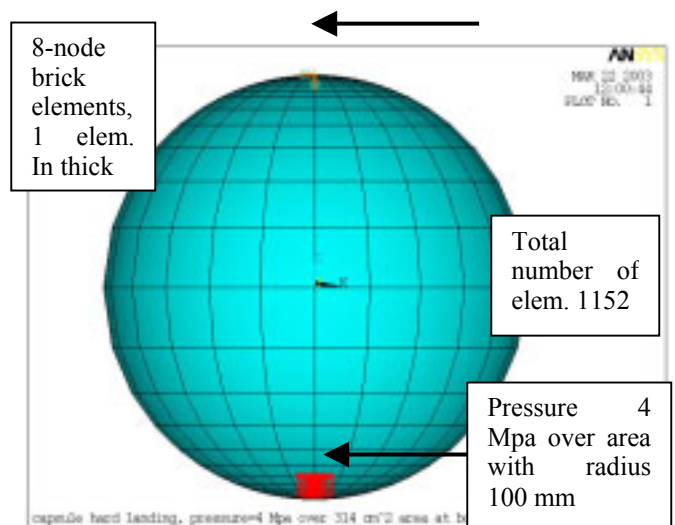


Figure 31. Case 3 Hard Landing, pressure 4 Mpa

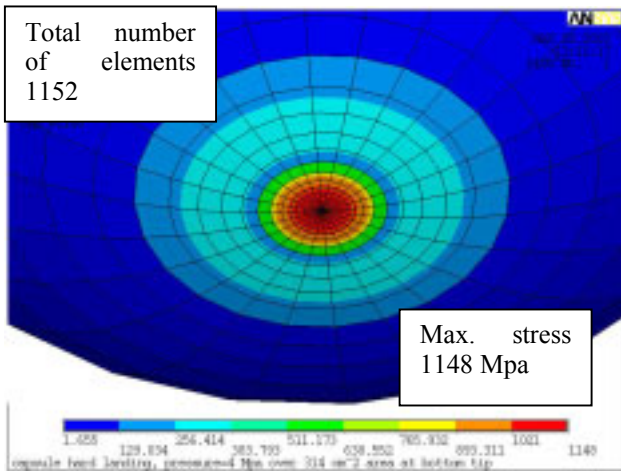


Figure 32. Case 4 Parachute Deployment Dynamic Loads

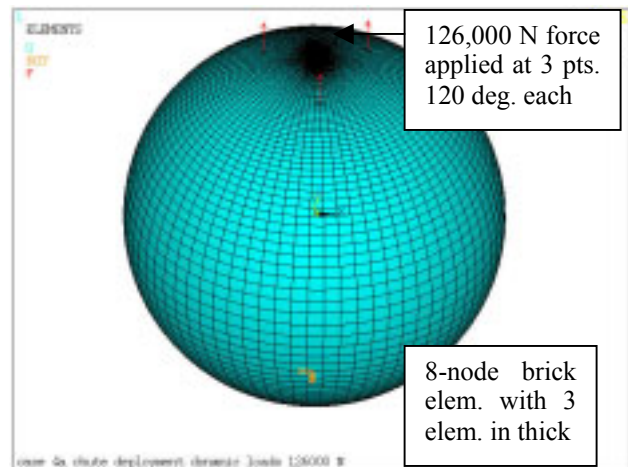


Figure 33. 29 Chute Deployment – Dynamic loads 126 000 N

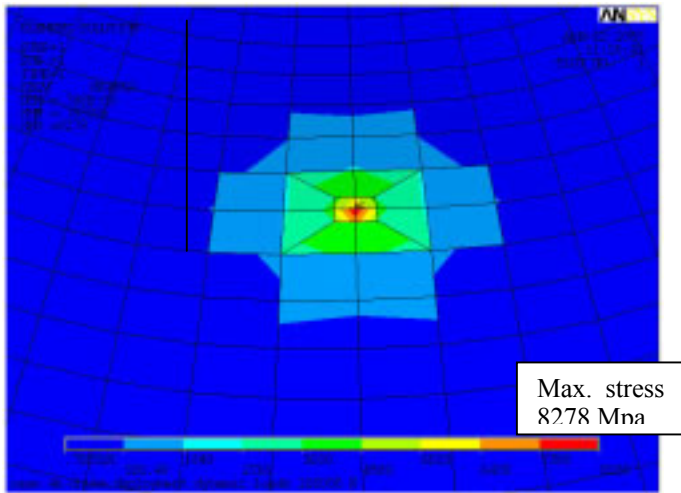


Figure 34. Von Mises Stresses near load applied point

Load case	Element Type	Element solution	Nodal solution	Total element number
Hard landing	brick	1148	1053	1152
Hard landing	brick	1096	1058	41472
Chute dynamic	brick	8278	6927	41472
Chute dynamic	plate	5993	5664	1152+

Table 7. Comparison of stresses from different model types and loads (stresses in MPa)

3.7.4 Stress Model Accuracy

According to Ansys documentation manual, finite element mesh are accurate enough when element stresses (non-averaged) are close to nodal stresses (averaged). For chute deployment dynamic load case, the maximum von Mises stress was 8278 Mpa based on element solution, while the nodal solution was 6927 Mpa, about 16% less than element solution. It seemed the mesh was still not fine enough around the concentrated forces. A model with plate element (SHELL63) was created to compare with brick element results. This plate element type model had 1152 elements plus some elements refined at near concentrated forces. Ansys has the capability to refine mesh for plate element (triangular and quadrilateral) and tetrahedron (4-node solid) in local area. The maximum von Mises stress was 5993 Mpa from element solution and was 5664 Mpa from nodal solution. The difference was only 5.5%. From above comparison, brick element model had higher stresses but larger variations between element and nodal solutions. The plate element model had lower stresses but with close solutions. The possible reason may be the aspect ratio (brick length/thickness) of about 40% of total elements in this model were greater than 20. Since each element had only 1 mm thickness but had more than 20 mm long in

length direction. Ansys Documentation suggests if the aspect ratio is greater than 20, the results would be inaccurate. Plate element is suggested by Ansys manual when the aspect ratio of brick element is more than 10.

Another concentrated force case, the hard landing case, was using the coarse model (1152 brick elements) in the analysis. This concentrated force, actually was a high pressure over a small area. The maximum von Mises stress was 1148 Mpa from element solution, while nodal stress was 1053 Mpa, which was about 8% lower than element solution. If the fine model with 41472 elements was used, the maximum element stress was 1096 Mpa, which was 3.5% higher than 1058 Mpa from nodal solution. This fine mesh had smaller difference but lower stress level. The above comparison is listed in Table 6.

3.7.5 Conclusions

Linearity exists in applied loads, thickness. If the loads change, the stress results and deformations will also change in linear proportion. So does for shell thickness.

Deformations for all cases are under 10^{-5} mm, which are relatively small compared to structure dimensions. Generally speaking, it is not needed in design consideration.

For soft landing case, the contact area between air bag and capsule shell is larger than that of the hard landing case, therefore stresses should be lower than hard landing case. This will be executed in the next step.

For chute deployment dynamic load case, stresses are very high around those three load applied locations, about 8278 Mpa (1200 Ksi). These loads are applied directly on the shell structure without any reinforced ring. These loads should transfer to the shell through this ring with some strong designed lugs. Additional reinforcements are required, as data clearly points to the failure scenario. We also considered extreme loading scenario, as parachute deployment time can be controlled to last over 10 sec, thus reducing loads by a factor of 5 to 10.

For most capsule areas, a shell of 3 mm thick steel are over-designed, except at bottom impact area and chute attachment areas. The maximum stress near impact the zone at bottom is 1148 Mpa. Utilizing the linearity relationship, the required thickness near impact the zone can then be calculated. Data points to mechanical failure scenario (for given model assumptions).

The stress results from 8-node brick elements cannot reduce the difference between element stresses and nodal stresses in the chute deployment case. Even the mesh is already very fine. The possible reason may be the higher aspect ratio (greater than 20) of many brick elements among these models. Ansys manual suggests under this situation it can be improved by using plate element. Because the maximum stress obtained from the brick model is 28% higher than that from plate the model, the results can be conservatively adopted. Considering the thermal analysis when thermal protection system is included in the future, brick element is still necessary.

Future stress analysis work will focus on composite materials (that have much higher yield strength) and anisotropic stress properties. Thermal analysis will be combined with stress analysis to account for thermal stress component and ANSYS LS-DYNA drop model will be utilized to study material deformation during hard parachute landing and soft airbag landing impact.

3.8 System Design, CAD and Integration

The engineering team working on the Wild Fire MK VI™ vehicle faces the formidable challenge of developing a brand new rocket design in a very short period of time. This challenging task is compounded by the small size of our dedicated engineering group. It is of critical importance to our effort to make each of our team members maximally productive. In order to maximize the productivity of each of our team members, we are making use of the latest in mathematical and CAD software, and building an interface to move information across the different platforms in the most useful way possible. Through careful design of our engineering process and tools, which we employ in our analysis, we are developing a tightly integrated engineering platform.

Our analysis process involves three major parts; simulation, finite element analysis, and analytical solutions carried out manually as verifications. Our design process involves an overview, or system, level of design, combined with a detailed design being developed with the aid of CAD software. By combining these three tools into one larger system the team expects to achieve very rapid design convergence. This means that at any time during our design process, if the design or flight envelope of the mission is changed, the entire analysis and engineering ready CAD model are updated and optimized for the new conditions.

3.8.1 Integration Methodology

The method by which integration of the engineering effort is accomplished plays a significant role in its overall effectiveness. Two paths lay open to any engineering effort engaging in the use of such a process; either to manually transfer data from one level of analysis to the next or to automate the task by using software to move said data across the different levels of the process. Each of these has its advantages, and can be applied in varying degrees and combinations.

Manually linking analysis and the model (Figure 35 at Right) and moving data across under direct supervision of the designers adds an extra layer which can lead to the detection of analytical errors. However, this same process increases the chance of human error in transferring this information from one body of work to another. An integrated system (Figure 36 at Right) prevents such errors, especially where there are many critical parameters affecting a design. At the same time, intelligent design of the system permits its users to account for the source of any parameter, and quickly track errors to their source.

For the purposes of the da Vinci Project, the engineering team is moving towards the extreme end of software level integration. This decision is being influenced by the desire to maximize the productivity of each team member, and to maximize the speed of the entire engineering process while balancing the available human resources. This level of integration means that any updates made by an individual team member at the particular level where he/she is working, i.e. analysis, flight simulation, or detailed design, will carry through the entire design, from the source of the change right through to the engineering drawings. The thin arrows (Figure 36 at Right) depict software interfaces which move data directly between the separate bodies of engineering work.

Our process begins at the CAD level [15], where a fully parametric model of our design is being constructed. This means that all the dimensions in the model are constrained relative to each other in such a way that the model maintains self-consistency even when parameters are changed. This model serves simultaneously to flesh out the design as it is brought to its final form, as well as to provide hard information about the design such as part masses and moments of inertia. This information will serve useful as we expand this integrated process to include feeding these parameters directly back into the simulations and analytical calculations.

Control of these parameters is accomplished via a spreadsheet, enabling external modification of the parameters. This step is where the CAD model becomes accessible to the entire engineering team, particularly those members who are not CAD users themselves. The parameters are all named and identified by the parts to which they belong, allowing anyone who has done analysis to link these parameters to their analytical work. Since some parameters depend on calculated values, such as a wall thickness needed to withstand a particular load, linking these parameters to analytical work leads to a great reduction in the number of controlling inputs that actually affect the design.

By driving the parameters directly from the calculation spreadsheets, a great increase in the efficiency of the modeling process is achieved. The model no longer needs maintenance when an engineer decides that a particular component needs to be re-analyzed for a different load case, he must simply carry out the analysis and link it to the actual parameters which control the part.

Process Control System for Rocket Design:

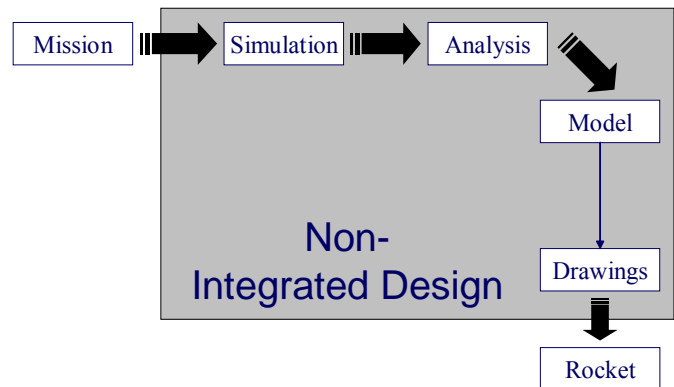


Figure 35. Manually linked analysis and modeling

Process Control System for Rocket Design:

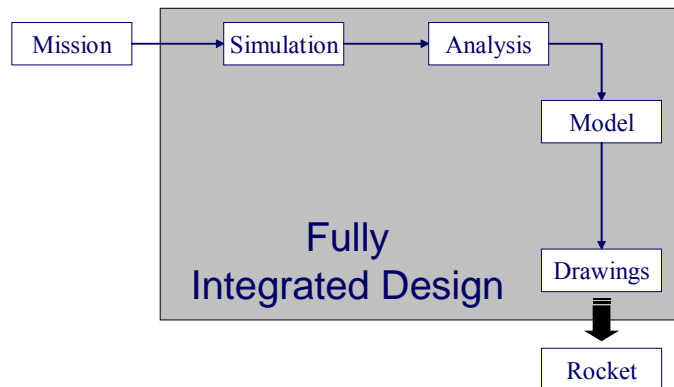


Figure 36. Software linked analysis and modeling

3.8.2 Results

By performing our analytical work on the computer, in a general form, we ensure the reusability of our analytical work and calculations despite possible changes in the operating conditions. Barring changes so radical that they require re-design of the spacecraft, variations in the mission profile's parameters will automatically cause the adaptive model to update itself and to meet the new criteria.

This open-ended modeling approach has linked our engineering drawings directly to our analysis, and creates engineering readiness across the entire spacecraft design. By rapidly designing components and subsystems, leaving the analytical details for later, the time needed to design the spacecraft is greatly diminished. In doing this, our team maintains an overview of the entire design, before digging in and carrying out the meticulous analysis that will specify the fine details of the design. As detailed analysis is completed, it is simply linked to the relevant parameters on the model, and the output drawings take one more step towards being complete.

An example of the power of reducing the number of free parameters is the primary fuel tank. It is constrained only by the volume of fuel it is to carry, and the pressure at which the fuel is to be stored. From these two mission dependant values, the entire tank analysis is carried out, and the entire design is specified. These two values affect everything from valve thickness and mounting strength to the geometry of the framework supporting the tank.

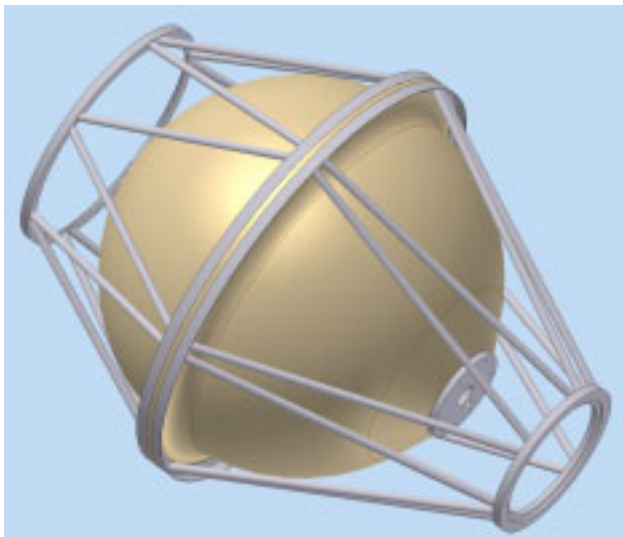


Figure 37. Primary fuel tank

Process Control System for Rocket Design:

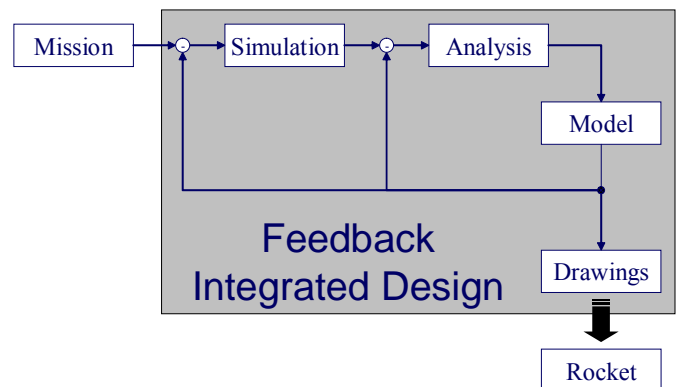


Figure 38. Feedback Integrated Approach

3.8.3 Summary

Lying before us is the task of completing the integration of our engineering process to include automatic feedback from the completed model back into the original analytical work (Figure 38). This is to be done by taking information including part masses and moments and transferring them in a fully automated way back to our simulators and analysis calculations. By extending our integrated process to this level, our team will be able to automate a large portion of the iterative refinement, which is of great importance to the completion of a good design. The benefits of this design approach are having a positive an impact on our team's productivity, and will continue to do so as we move steadily towards the completion of the project.

The team has developed an effective and streamlined engineering process which is leading to definite increases in our productivity. By using a parametric CAD model, we are ensuring open-endedness in our design while still making definite steps towards its completion. By controlling the model parameters from spreadsheets we are making the design accessible to all members of the engineering team. By linking our analysis directly to the parameters, we are maximizing the power of the parametric model, while reducing the number of free parameters that are affected by mission level decisions. Distributed work environment (email server, interactive document sharing and real time message exchange) is implemented with support of Ramius Corp (see Figure 39). From the combination of all these elements we have full engineering readiness in all parts of the design where analysis has yet to be completed.

This fruitful combination of extensive integration and engineering readiness give our team the ability to bring each member's capacity fully to bear on the great challenge of developing a manned craft in a very short time.

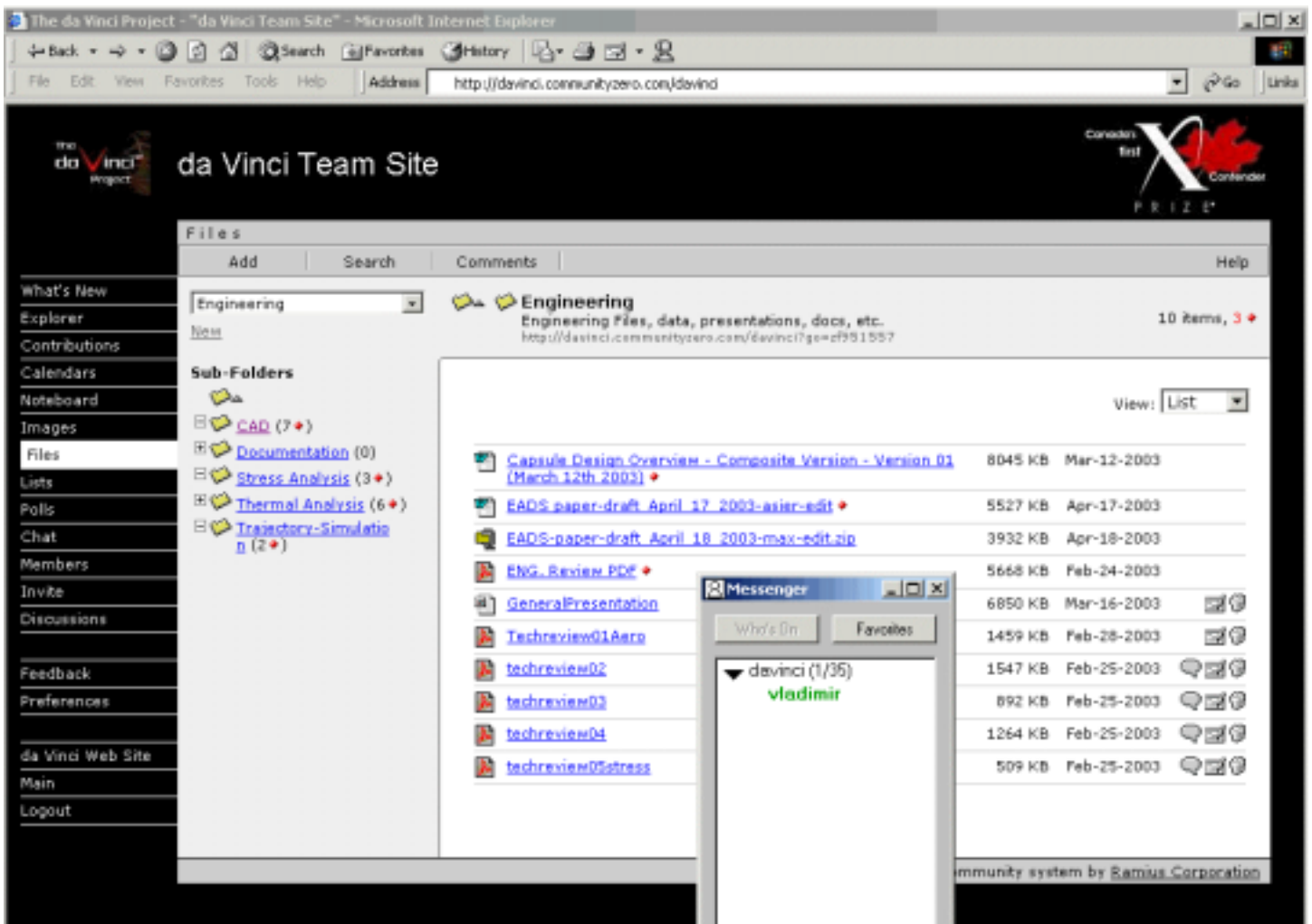


Figure 39. Distributed work environment and document sharing on RAMIUS Server (<http://davinci.communityzero.com>)

3.9. Ground Operations Considerations

In addition to being able to function in the spaceflight environment, the spacecraft must also be able to withstand the rigors of transportation, ground handling, setup & preparation for launch, and recovery. The structural rings at the circumference of the fuel tank and the base of the aero-shell provide structural support to allow the Propulsion Section to rest on its side, on a sufficiently level surface, without damage to the aero-shell. These rings also carry the attachment points by which the Propulsion Section can be lifted, handled, and secured for transportation. The spacecraft will be supported during transportation, handling, and maintenance, by a protective ground handling cradle made of tubular steel. This cradle will have tie down points matching those on the spacecraft, allowing the spacecraft to be secured to the cradle using straps, clamps, or bolts. The cradle will have removable casters to allow simple movement by hand under shop conditions. For transportation, the cradle can be hoisted onto a truck and secured there, without touching the spacecraft itself. For recovery from the landing site, the spacecraft can be rolled onto the ground handling cradle from its rest position. In this maneuver, the ground handling cradle is placed beside the Propulsion Section, and a winch on the recovery vehicle is used to roll the Propulsion Section onto the cradle. The structural rings at the fuel tank and aero-shell base support the propulsion section through this maneuver. The ground handling cradle can then be winched onto a low-deck flatbed trailer, avoiding the requirement for a crane or helicopter to recover the spacecraft. Similar ground handling and recovery procedures are used for the Capsule. The Propulsion Section ground handling cradle can accommodate the integrated spacecraft (i.e. Propulsion Section with Capsule in place) for ground handling and transportation. For recovery, a separate ground handling fixture will be used, which is designed to hold and support the spherical Capsule. The exact landing sites of the two spacecraft components and the balloon depend on both the winds at altitude – which will be known before launch – and the surface winds in the landing area, which will be less well known. Recovery crews will be guided to the landing sites by a Recovery Telemetry System which combines a GPS receiver, a digital radio link to the Mission Control Center, and mapping software. The system displays in real time the recovery vehicle's current position, the spacecraft components' current positions, and the estimated landing site (determined by simulations per Section 3.1)

superimposed over a local road map on a screen in the recovery vehicle. Unique operating procedures and ground support equipment are being developed for our unique combination of a large balloon and heavy manned payload. The launch procedure and equipment are based on those used for large scientific balloons, using a specially designed launch cradle attached to a truck, and a weighted roller for control of the balloon in surface winds of up to about 12km/h. Figure 40 shows the arrangement of the spacecraft and InterSection Adapter during launch. The spacecraft's launch cradle is mounted on free-steering casters and rigidly attached to the front of the vehicle. As the balloon and InterSection Adapter rise, the vehicle is maneuvered to keep the spacecraft directly beneath the InterSection Adapter until it is lifted off the cradle

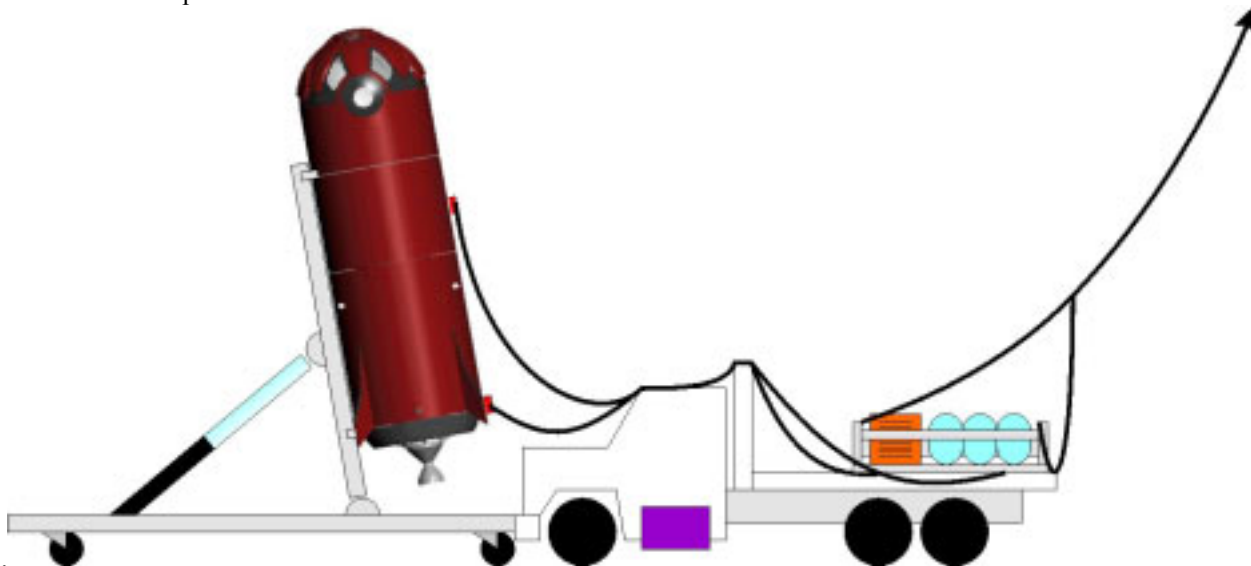


Figure 40. Vehicle Arrangement for balloon launch

Special handling procedures must be observed during recovery of the balloon on the ground, as well as during routine handling and inspection of the balloon. The recovery procedure and equipment are based on those used for hot air balloons. Once laid out on the ground, the balloon will be bundled into a specially designed protective transport container, by a procedure which minimizes manhandling and eliminates dragging. After recovery, the balloon will be laid out for inspection and repair in a facility that has been kept clean and free of debris that could puncture the envelope.

4.0 CONCLUSIONS

The entire spacecraft consists of a small number of subsystems, and has been designed to maximize simplicity, safety, and redundancy in all respects. By keeping the rocket as basic as possible, the design team feels there will be fewer modes of failure than with larger and more complex launch systems. This back to basics design philosophy will also serve us well in the race to complete our spacecraft, as we aim to use proven technologies that have a track record and a large body of experts whom we can tap. The Wild Fire Mk VI™ balloon launched spacecraft demonstrates the simplicity and low cost that can accompany safe space flight when unconventional technologies are matched in a new and effective way.

With the recent completion of our initial research and development phase, the team's efforts are now focused on the detailed design of the spacecraft. Manufacturers of systems such as parachutes and airbags are being researched and approached, and detailed analysis work is being carried out on every aspect of the design. The team aims to begin construction and testing of spacecraft components as by early summer, with a balloon test launch of the capsule by the middle of the season. This major milestone will demonstrate both our launch strategy of being carried aloft by a balloon, as well as serving to fully test the landing systems of the capsule, including its passive stability, parachutes, and airbags. With steady progress and the successful completion of this milestone the team will be poised to rapidly complete its mission, and to win the new race into space.

The da Vinci Project is as much a technology achievement as it is about Inspiration and Education in Space Science & Technology Achievement and Overcoming Barriers. The non-science aspect or overcoming barriers is an important one. It can be manifested in many different ways to the audience to inspire youth that all barriers can be overcome and that they are for the most part reinforced by our inability to look past ourselves. The da Vinci Project's greatest non technical achievement will be overcoming the psychological barrier to space flight for the common man. It will be as lasting an accomplishment as the Lindbergh flight. The beauty is how it can be applied to all aspects of life. The education effort will emphasize making the Project's achievements of interest to the widest possible audience.

The da Vinci Project emphasis on Space Science and Technology will include demonstrated breakthroughs in cost and safety sensitive reusable propulsion, structures, thermal and recovery systems. The da Vinci Project has taken ground breaking steps working with government for launch approval of private sector manned space flight and overall civilian safety. Indeed the first sponsor of the da Vinci Project was the oldest legal firm in Canada - Blake, Cassels and Graydon who are working with us on the pioneering of regulations governing the safe execution of this emerging industry.

To learn more, ask for our comprehensive Partnership Document, visit www.davinciproject.com or the X Prize official website at <http://www.xprize.org>. For a presentation and video please contact Brian Feeney, Team Leader at 416.434.7470 bfeeney@davinciproject.com

ACKNOWLEDGMENTS

Authors would like to acknowledge help of Jennifer Sutton (Technical Documentation Specialist) and of Greg Elliot, Chris Johnson and Khal Shariff (Graphics and Web Design), Mr. Tony Lee (Project Management) and Mr. Guillaume Tremblay (flight analysis).

REFERENCES

1. David E. Fisher, M.J. Fisher, X-Prize, Discover, vol.23, no.7, July 2002, p. 50-57
2. Racing for Space with the X-prize, National Geographic, May 2001
3. B. Feeney, V. Kudriavtsev, Aeroheating Analysis for DaVinci Space Project Ballute, ORVA Corp (Toronto, Canada), <http://www.cfdcanada.com>, Prepared for ASME Int. Symposium on Computational Technologies for Fluid/Thermal/Chemical Systems with Industrial Applications Atlanta, Georgia, July 22-26, 2001, USA
4. Lynn Lansford, A Private Space Race, Wall Street Journal, February 5th, 2003
5. M. Strobel, No space for fear, The Toronto Sun, Feb. 4th, 2003
6. R. Hercz, Out of this world, Toronto Life, May 2003, p.71-80
7. Preston Lerner, A Few Dreamers Building Rockets in the Workshops (Other Contenders), page 64, Popular Mechanics, May, 2003
8. CFD-FASTRAN Manual, CFDRC, www.cfdrc.com, 2002
9. CFD-ACE+ Manual, CFDRC, www.cfdrc.com, 2002
10. ANSYS 7 Manual, www.ansys.com, 2002
11. B.R. Hollis, J.N. Perkins, Transition Effects in the Wake Heating of a Blunt Body, AIAA 97-2569
12. N.F. Krasnov, Aerodynamics, Vishaia Shkola, p.1-629, 1971 (in Russian)
13. B.M. Pankratov, Basics of Thermal Design for Space Transportation Systems, Mashinostroenie, p.1-1-303 (in Russian)
14. W.T. Thomson, Introduction to Space Dynamics, Dover, N.Y., 1986, p. 313
15. S. Tickoo, Autodesk Inventor for Designers, R.6, CADSIM Technologies, p.1-768, <http://usa.autodesk.com>
16. Ben-Yakar, A., and Gany, A, Hybrid Engine Design and Analysis, AIAA Paper 93-2548, 29th AIAA/ASME/SAE/ASEE Joint Propulsion Conference, Monterey, CA, June 28 - July 1, 1993
17. A. Heslouin, et. al, Propulsion of Microsatellites by Hybrid Rocket Engines, <http://www.ee.surrey.ac.uk/SSC/H2O2CONF/foucaud.htm>
18. M. Dornheim, Flying to Space for Low Cost, Aviation Week and Space Technology, April, 2003